BIOACTIVE NANOCOMPOSITES FOR DENTINOGENIC RESTORATION

An honors thesis

Submitted by

Lauren Nadkarni

In partial fulfillment of the requirements

For the degree of

Bachelor of Science

In

Biomedical Engineering

May, 2009

Adviser: Professor David Kaplan, Ph.D.

Acknowledgments:

Thank you to Aneta Mieszawska for providing excellent mentorship and guidance in addition to some laboratory materials (DNA plasmids) for this study.

Thank you also to David Kaplan and the Tufts BME Department for providing tremendous mentorship, assistance, and support for this study.

`

Table of Contents:

`

`

Table of Figures:

`

Abstract:

Restoration of bone after injury or decay is essential. This is especially true for teeth; when the pulpo-dentin complex is damaged, dentinogenic repair may alleviate the pain and restore functionality of the tooth. There are two current mechanisms of repair: root canals and bioactive molecule implants. Removal of the dental pulp in a root canal procedure eliminates functionality of the tooth and is costly. Bioactive molecules, such as inorganic glasses or cements, have inconsistent material properties with the target tissue. Therefore, novel bioactive nanocomposites were developed to restore dentin and tooth function after injury. The nanocomposites were two-dimensional chimeric protein films comprised of a domain containing repeating sequences of spider dragline silk for strength and stability and a domain containing either an R5 or A3 silica precipitating sequence for biomineralization capabilities. We hypothesized that the varying number of silk repeating sequences, in combination with insertion of each silica precipitating sequence, would differentially precipitate silica and therefore affect the biomineralization capabilities of human mesenchymal stem cells (hMSCs) *in vitro*. Scanning Electron Microscopy (SEM) imaging techniques were used to characterize the protein films which had undergone silicification reactions with pre-hydrolyzed tetramethylorthosilicate (TMOS) in HCl with or without 60% (v/v) glycerol. Light microscopy techniques were used to confirm that hMSC cells were differentiated in osteogenic media with films cast on tissue culture plates throughout a two-week cell study. Energy dispersive X-ray spectroscopy (EDAX) analysis confirmed the deposition of calcium phosphate, a hydroxyapatite precursor and major organic component of bone. Cell viability and gene expression analysis of 3 important genetic bone markers (bone sialoprotein, BSP, alkaline phosphatase, ALP, and collagen type I, ColI) was performed with Alamar Blue, PicoGreen, and qRT-PCR assays. The protein films successfully

`

precipitated silica particles on the surfaces after silicification reactions were performed. The particles ranged in size from 200-400nm and were separated (as opposed to agglomerated) on films treated with glycerol. Protein films were successfully cast on tissue culture plates and seeded with hMSCs, which differentiated toward osteoblasts when cultured in osteogenic media. The cells were viable and showed osteoinductive properties, although the gene expression results were somewhat inconclusive. Cells seeded on protein films with silk and silica sequences deposited more calcium phosphate on the surface of the films and silica particles than cells seeded on the tissue culture plate alone. Overall, we achieved our specific aims of precipitating silica and characterizing the chimeric protein films based on their sequences and successfully differentiating hMSCs towards osteoblasts that deposited materials characteristic of biomineralization.

`

Background and Introduction:

Dental decay and loss of function with inadequate restoration material leads to increased pain and suffering, frequent need for root canal surgery, and high costs of dental work. Severe injury or decay can necessitate complete removal of the dental pulp by a root canal procedure, thereby reducing the natural functionality of the tooth. According to the American Association of Endodontists, nearly 16 million root canals are performed each year, and the procedure can cost between $300 and $1000 per tooth (www.AAE.org). It is known that dentinogenic restoration can be achieved using various bioactive molecules, however the mechanisms are poorly understood (Goldberg and Smith, 2004). The current inorganic restoration materials, such as bioactive glasses and composites, are ill-suited for the task; they are often brittle, have mechanical properties inconsistent with the target tissue, and have decreased stability at the bone/engineered material interface (Ndahi, 2001 and Oliveira, et al., 2003). Furthermore, these materials still fail to restore full functionality to the tooth after implantation. Therefore, a new, better bioactive material is needed to improve and better understand the bone restoration process after injury or decay.

Teeth with diseased or damaged dentin and pulp cause pain and can be costly to repair. If the damage is severe enough, a root canal procedure or extraction may be performed; these are painful procedures that excise damaged dental pulp and replace it with a biocompatible rubber, resulting in weakened or lost function. As a replacement for root canals and extractions, bioengineered dentinogenesis may provide a permanent solution for repairing damaged teeth *in vivo*. However, current engineered dentinogenic techniques require implantation of inorganic materials that are brittle, inconsistent with the target area, and have insufficient stability.

`

Dentin, located beneath the enamel and cementum of the tooth, is a hard, chalky tissue similar to bone. It contains tubules, dentinal fluid, and intertubular matrix, and is highly mineralized (Kaplan, 2007). 74% of dentin is mineral (including hydroxyapatite), and a majority of the organic components is type I collagen (Duailibi, 2006). Dental pulp, the fibrous connective tissue situated directly below the dentin, contains blood vessels, nerves, and lymphatic tissue, which combine to provide nutrients to the dentin and sensation to the tooth. As shown in figure 1, the pulpo-dentin complex is intricate and dynamic; the pulp and dentin must work together in order for the tooth to remain healthy and functional. Dentin is a poor barrier to external irritants, but the pulp reacts to noxious infiltrations by physiologically fortifying the dentin (Pashley, 1996). For example, the pulp can respond to irritation by becoming inflamed or initiating dentinogenesis to repair the damaged area. When decay or damage of the dentin and pulp occurs, the tooth may become infected and cause severe pain. The most common solution to this problem is a root canal, a procedure by which damaged dental pulp is removed and replaced with inorganic fillers. Current engineered repair mechanisms involve implanting biocompatible, antibacterial inorganic materials in the damaged site, but these techniques introduce a surface that has inconsistent mechanical properties, decreased stability, and involve a loss of function.

`

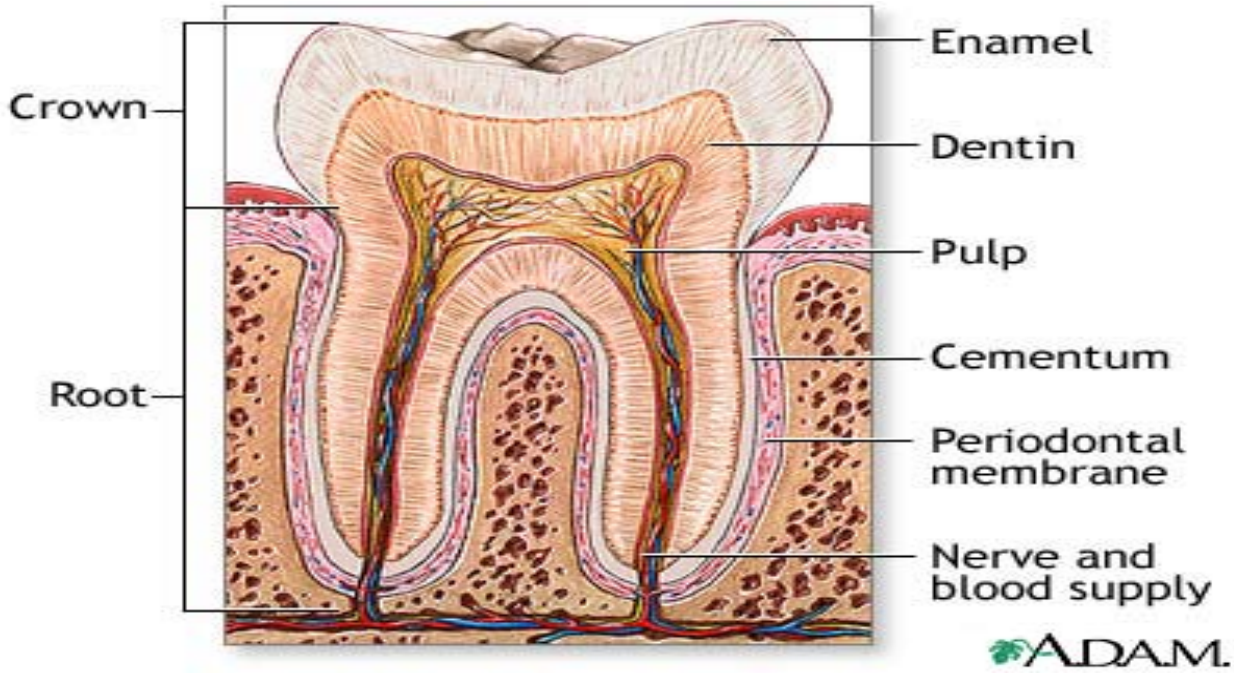

Figure 1. Tooth structure demonstrating location and components of pulp and dentin (www.nlm.nih.gov/medlineplus/ency/images/ency/fullsize/1121.jpg)

Silk fibroin isolated from silkworm cocoons of *Bombyx mori*, the domesticated silkworm, has been used as a scaffold in numerous tissue-engineering applications. It is biocompatible, biodegradable, readily available, and can essentially be substituted for collagen in tissue constructs. In 2005, Wang et al. used 3-D aqueous-derived silk scaffolds to produce engineered cartilage *in vitro*, which is typically largely made of collagen. They achieved cell arrangement in the silk scaffolds, mimicking that of native cartilaginous tissue, which elucidated the potential of using silk as a scaffold. In 2006, Marolt et al. successfully created bone and cartilage tissue constructs based on silk scaffolds, which have the potential to serve as models for other types of tissue engineering scaffolds. On the commercial level, companies like Serica Technologies, Inc. and Neurotex, Ltd., are investigating the use of silk fibroin engineered scaffolds for cartilage, ligament, and nerve regeneration, for example in anterior cruciate ligament (ACL) replacement.

`

Silk fibroin scaffolds provide strength and stability to the damaged area, supporting the proliferation of new tissue-specific cells and then biodegrading to leave behind natural, "home grown" functional tissues.

Achieving mineralization is a desirable goal for many biological processes, including bone formation. Dentin shares many characteristics with bone, and mineralization is also an important component of dentin restoration. Biomineralization is defined as the biological guidance and oversight of oriented crystal growth. Although the mechanisms of mineralization in dentin are still unclear, the organic matrix has been found to play a large role (Narayanan et al., 2001; Ye et al., 2004). In addition to calcium, one of the main components required for mineralization in the pulpo-dentin complex is silica. In nature, many sponges and diatoms produce silica, SiO_2, and use it as a structural material. Silica is also produced in some protozoa and plants as well (Perry, 2001). One class of diatomic proteins, called silaffins, has been found to promote rapid silica precipitation *in vitro* (Lopez et al., 2005). It is believed that silicatein, shorthand for *silica* pro*tein*, serves as a catalyst for silica formation, especially in diatoms.

Silicatein protein production must be controllable, reproducible, and regular in order to consistently obtain desired protein characteristics. In 2000, Cha et al. developed a technique for producing these proteins and demonstrated the ability to modify silica protein from the sponge *Tethya aurantia*. In their study, cysteine-lysine block copolypeptides were created to mimic silicatein properties and self-assemble in ordered morphologies. The cysteine sulfhydryl (SH) groups on the polymer were oxidized and reduced to change the structure of the protein. The polymers formed hard spheres and defined columns of amorphous silica in a controlled pattern. This study showed that specific treatment of the peptides achieves controlled, regular, and predictable proteins. Importantly, specific peptides could be manipulated in a regular way to

`

create a reproducible protein with desirable properties. The techniques used are applicable to other proteins as well. Controlled silica formation can be used as a basis for further mineralization by recruiting factors necessary for the processes to occur. Therefore silica not only offers stability, but also provides a location for mineralization of other materials in the pulpo-dentin complex.

In 2002, Kröger et al. extracted native silaffins from diatoms. The proteins remained undamaged and could be studied as they exist in nature. The study also showed that specific post-translational modifications are important for proper biological function and activity. They detected a silaffin-silica phase *in vitro*, which may represent a building material for diatom biosilica. In 2003, Knecht and Wright noted that a repeating motif sequence in silaffin promotes active silica formation. The R5 sequence from sil1p proteins, as shown in figure 2, will be examined further in the proposed study as it was found to have an important role in silica precipitation processes.

`

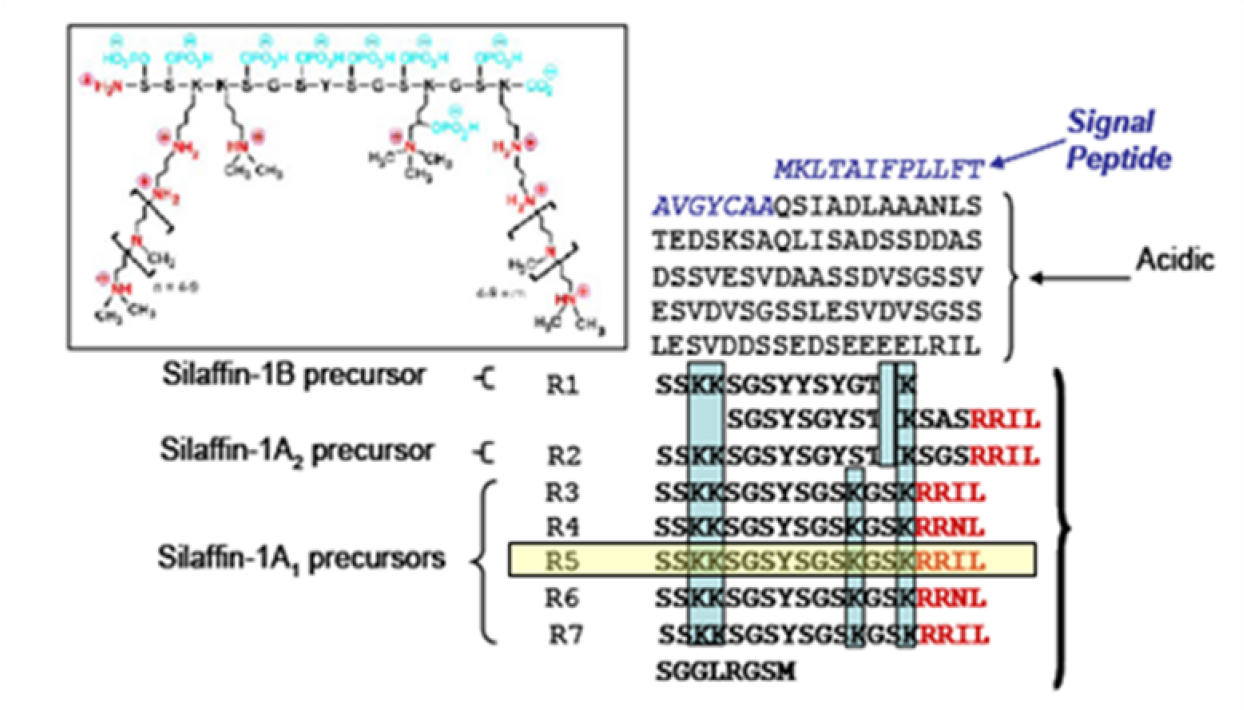

Figure 2. Primary structure of sil1p protein from silaffin. The location and sequence of the R5 repeat is highlighted.

(Kaplan, David. 2006. NIH Silica Application (R01 DE017207-01A1)

Chimeric proteins are often used in biological research and therapeutics because they can combine several desired properties and functions in one protein molecule. Chimeric proteins, also called fusion proteins, are engineered proteins created by splicing together several gene sequences that originally coded for separate proteins, and then expressing these sequences together. When the chimeric sequence is translated correctly, a single oligonucleotide is produced with functional properties corresponding to the original proteins. As with any engineered protein of interest, the sequence can contain a tag that is useful for tracking in subsequent manipulations of the protein.

Biomimetic approaches to biosilica formation have been proposed. In 2004, Foo et al. controlled biosilica structure morphology through physical and chemical manipulations, producing predictable, regular forms as shown in figure 3. In 2006, they showed that protein

`

sequence, treatment, and silica-precipitating (silicification) reactions all affected silica production on protein films Also in 2006, Kaplan used a specific procedure to produce chimeric proteins *in vitro* which was used to sustain protein production for this study. Figure 4 is an overview of the procedure used to clone a specific sequence in E. coli for the expression and purification of desired proteins.

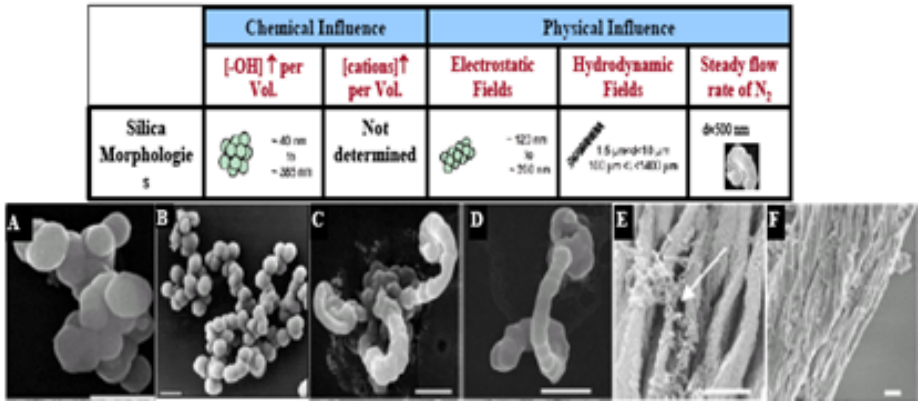

Figure 3. Chemical and physical influences on silica morphologies (image from Foo et al., 2004).

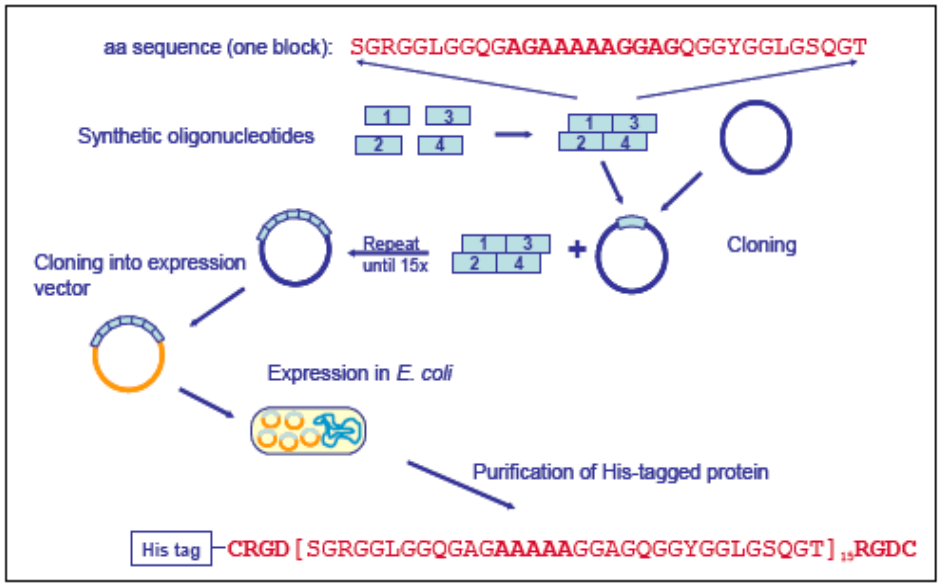

Figure 4. Outline of the procedure used to clone a desired sequence. Here, a consensus repeat of spider dragline silk is cloned in *E. coli* (image from Kaplan, 2007)

`

This study was conceptually grounded in a combination of technologies and knowledge about the scaffold properties and strength of silk and the mineralization capabilities of silica with applications in dentinogenic restoration. Spider dragline silk from *Nephila clavipes*, a golden orb-web spider, was used due to its great tensile strength and mechanical properties. In fact, silk is the strongest known natural fiber. Past research has been unable to address the problem of an incompatible dentin-pulp-engineered material interface due to the complexity of the pulpo-dentin complex. Therefore, we proposed a new material that contains biocompatible dentin and pulp properties with functional attributes. These novel classes of fusion proteins had two domains: a spider dragline silk sequence (SGRGGLGGQGAGAAAAAGGAGQGGYGG-LGSQGT) and a silica-forming silaffin sequence (either R5: SSKKSGSYSGSKGSKRRIL or A3: MSPHPHPRHHHT), and were studied in two dimensions (2-D) as chimeric protein films.

Our preliminary results show that a silk/silica construct can be designed with specific control of the material's design and functional properties. This is important because controlling the surface morphology of tissue engineering constructs may be achieved by modifying the sequences of the proteins used to make the scaffolds. The differences in morphology and biomimetic properties of the engineered silk/silica protein films are related to the scaffolds' ability to support cells *in vitro*. For example, rough, irregular surface textures provided increased cellular attachment for osteoblast-like cells, possibly because of the increased surface area for attachment (Bowers, et al, 1992). Therefore, films that precipitate silica, thereby creating non-smooth surfaces for cell attachment via surface modifications, may have an increased ability to support cells *in vitro*.

For this study, we used human mesenchymal stem cells (hMSCs) to determine the ability of the protein films to promote osteogenesis. hMSCs have been shown to differentiate into a

`

variety of cell types, including chondrogenic and osteogenic cells. In 2003, Chen, et al. demonstrated that hMSCs could adhere, spread, proliferate, and produce collagen matrix on arginine-glycine-aspartic acid (RGD)-modified silk scaffolds. Although this work assessed chondrogenesis and not osteogenesis, the success of this study provides biological plausibility that osteogenesis is possible as well.

Osteoinductive properties are assessed by standard methods including cell viability assays, double-stranded DNA (dsDNA) content, and quantitative RT-PCR genetic expression analysis. There are several standard genetic markers that can be used to assess the osteogenic capabilities of the cells. In 2004, Meinel, Karageorgiou, Fajardo, et al. showed that hMSCs demonstrate the ability to undergo osteogenesis *in vitro* on hexafluoro-2-propanol (HFIP)-derived silk scaffolds. For three dimensional (3-D) silk scaffolds, there is conflicting evidence about whether aqueous-derived or HFIP-derived scaffolds better promote osteogenic responses, so it is important to confirm hMSC osteogenic capability in 2-D silk scaffolds (Kim, et al., 2005). Additional studies showed that hMSCs cultured in osteogenic medium had higher expression of bone sialoprotein, osteopontin, osteocalcin, and bone morphogenetic protein 2 (BMP-2), all significant genetic markers for bone formation (Meinel, Karageorgiou, Hofmann, et al., 2004 and Meinel, et al., 2005). However, the osteogenic medium contained BMP-2, and therefore more studies must be done in to determine whether bone formation or precursors can arise without the addition of BMP-2 in the osteogenic medium.

For this study, measurements included expression of bone sialoprotein (BSP), an indicator of the extent of mineralization; alkaline phosphatase (ALP), an enzyme that is found in remodeling bone; and collagen type I (ColI), the major organic component of bone. Marolt, et al. (2006) showed that the formulation of the media in which cells are cultured has a profound

`

effect on the ability of the cells to differentiate into a certain cell type. Adding chondrogenic versus osteogenic factors to the medium of the same population of cells caused formation of cartilaginous or bone-like tissue structures. They established a standard osteogenic medium containing DMEM with 10% FBS, 1% pen-strep, 0.1mM non-essential amino acids, 50μg/mL ascorbic acid-2-phosphate, 10nM dexamethasone, and 7mM β-glycerophosphate, which was used for this study.

The most important consideration for this cell study was the determination of whether the engineered protein films would support cell attachment, migration, cell-to-cell interactions, cell proliferation, and differentiation. Previous work has shown that silk RGD sequences, recognition sites for integrin-mediated cell adhesion, increase cell attachment of mammalian cells including bone marrow-derived stem cells (Sofia, et al., 2001, and Chen, et al., 2003). However, for this study, RGD sequences were not necessary because our preliminary results have shown that cells successfully attach to chimeric protein films with similar sequences. The similar sequences allows for versatile processing options to alter structure and morphology based on tissue-specific needs and provided structural support for cells during the stages after implantation (Wang, et al., 2006). Preliminary results show that this approach successfully achieves integration of cells with the bioactive nanocomposite toward osteogenesis. (Mieszawska, Kaplan, and Perry, 2009). Studying the cells on the engineered films for two weeks should be long enough to assess their proliferation, differentiation, and mineral deposition abilities in an effort to provide preliminary results indicating whether these films have osteoinductive properties towards eventual dentinogenic restoration *in vivo*.

`

Hypothesis:

In this study, we engineered novel silk/silica biomimetic nanocomposites to provide stability, biodegradability, and consistent mechanical and morphological properties at the site of implantation as a basis for dentinogenesis *in vivo*. Therefore, we hypothesized that alterations to the silk and silica domains of fusion proteins would produce different material characteristics, such as precipitated silica size and distribution as measured by SEM imaging techniques, due to dissimilar mechanisms of silica precipitation and the implementation of varied chemical influences, such as treatment with 60% (v/v) glycerol. Furthermore, these differences in nanocomposite properties should contribute to dissimilar cell characteristics such as cell viability, morphology, and gene expression as they relate to osteogenesis *in vitro*.

`

Specific Aims:

Our 3 main objectives for this research experiment were: 1) to assess the efficiency of creating silk fusion proteins with different combinations of specific silica domains. This was achieved by altering the silica domain (either R5 or A3 sequences) and varying the silk content (6mer or 15mer) of the fusion proteins. Since the sequences for each protein family were different, the fusion proteins should have different morphologies and extents of silica precipitation, as measured by SEM imaging techniques. 2) To identify relationships between and correlate the sequences of the fusion proteins to the morphological and silica precipitation properties. Optimization of the protein film properties is dependent upon the characterizations of each protein family, determined by SEM and EDAX analysis, so cataloging the specific properties was essential for future clinically relevant studies. And 3) to perform a 2-week *in vitro* cell study using hMSCs to provide some preliminary evidence of changes in osteoinductive properties over time based on the unique characteristics of the protein films.

`

Methods:

We cloned silk repeating blocks and silica precipitating sequences and sequenced them to confirm successful insertion of the vectors. The vectors were transformed into RY cells for protein expression and purified in a column using a Ni-NTA resin. The purified and dialyzed protein was dried by lyophilization and dissolved in HFIP to create a casting solution for the films. The films were treated with methanol to induce β-sheet formation and then underwent chemical treatments to precipitate silica particles. After confirmation of successful silica precipitation, hMSCs were seeded on films cast on 24-well tissue culture plates, cultured in osteogenic media for 2 weeks, and assessed for cell viability and genetic expression in tandem with morphological and chemical analysis of the films to evaluate the osteoinductive properties of the scaffolds.

Part I: Creation of fusion protein films

Figure 5. Schematic overview of the protein film protocol.

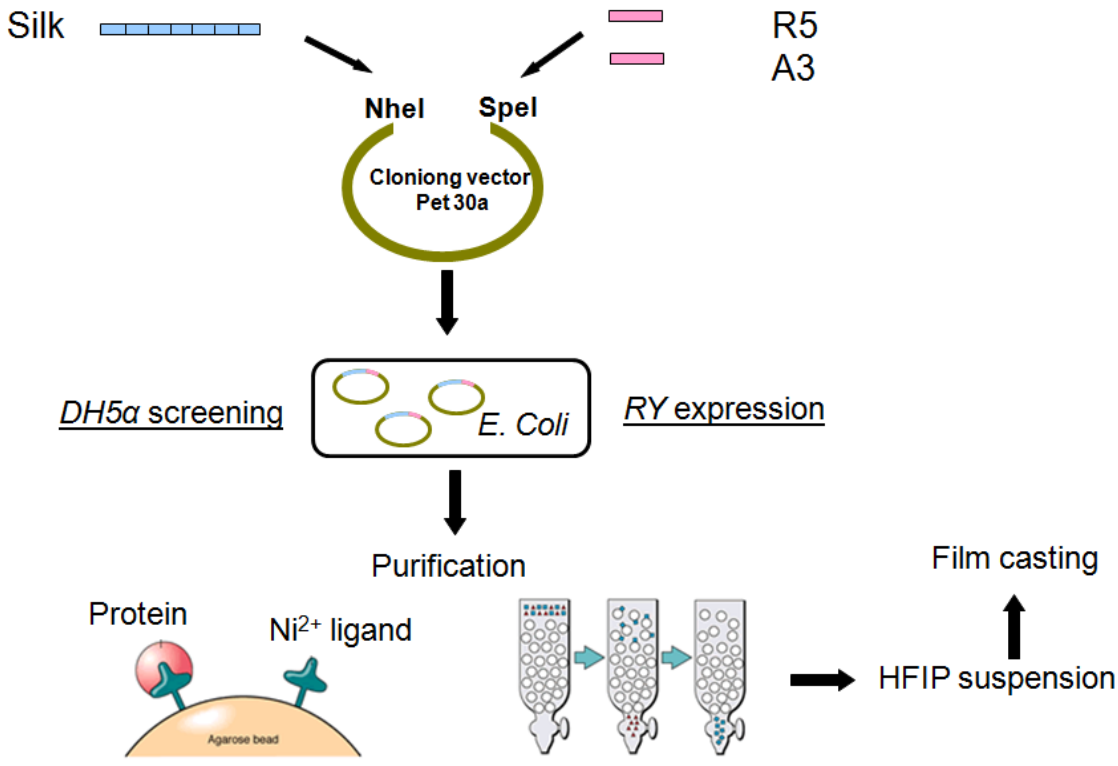

`

A) Vector and Insert Expression

i) Ligation:

Two silica sequences, R5 (SSKKSGSYSGSKGSKRRIL) or A3 (MSPHPHPRHHHT), were examined in combination with a silk sequence (SGRGGLGGQGAGAAAAA-GGAGQGGYGGLGSQGT) which was repeated 6 times (6mer) or 15 times (15mer). The proteins were thus labeled 6mer (no silica sequence), 15mer (no silica sequence), 6R5, 6A3, 15R5, and 15A3 herein. 4μL DNA vector (6mer or 15mer) was added to 1μL 1:20 dilution DNA insert (A3 or R5), 3μL dH_2O, 1μL T4 ligase buffer, and 1μL ligase and was then amplified in the thermocycler where the samples were incubated at 22°C for 30 minutes, 16°C for 16 hours, and then stored at 4°C.

ii) Transformation into DH5α cells:

Silk/silica fusion protein sequences were inserted and expressed in *E. coli*. Briefly, 50μL *E. coli* DH5α cells were added to 2μL pET vector (6mer or 15mer) on ice. The cells and DNA were left on ice for 30 minutes, and then heat shocked at 42°C for 90 seconds to insert the vector into the *E. coli* host. The sample was then returned to ice for 2 minutes. Then 900μL SOC media at room temperature was added and the samples were shaken in an incubator at 37°C for 1 hour. After incubation, the samples were centrifuged for 1 minute at 13,000 RPM, and 800μL of the liquid phase was removed. The pellet was then resuspended in the remaining 100μL liquid phase and plated on LB/ agar plates with kanamycin.

Overnight cultures:

5μL kanamycin stock solution was added to 5mL LB media to make a final concentration of 25μg/mL along with 1 colony of *E. coli* from the DH5α plate and shaken overnight at 37°C.

`

iii) Miniprep for Sequencing Analysis:

Plasmid DNA was purified using the QIAprep Spin Miniprep Kit using overnight cultures of *E. coli* DH5α cells in LB medium. Briefly, pelleted bacterial cells from the overnight cultures were resuspended in 250μL buffer P1 with RNase A. 250μL of buffer P2 was then added and mixed by inversion, making sure that the lysis reaction did not exceed 5 minutes. Then 350μL buffer N3 was added and mixed by inverting, producing a cloudy solution. The samples were then centrifuged at 13,000 RPM for 10 minutes. The supernatants were applied to the QIAprep spin column and centrifuged for an additional minute at 13,000 RPM. The flow through was discarded, and the spin column was washed with 0.5mL buffer PB, then centrifuged for 1 minute at 13,000 RPM. After discarding the flow-through, the spin column was washed with 0.75mL buffer PE and centrifuged for 1 minute at 13,000 RPM. The flow-through was discarded and the sample was centrifuged again with the same conditions. 40μL dH_2O was added to the center of the column, let stand for 1 minute, and then was centrifuged for 1 minute at 13,000 RPM to elute DNA for sequencing.

Sequencing:

We confirmed the sequences of the samples by sending them for analysis by the Tufts University Medical School in Boston, Massachusetts. Obtained sequences were analyzed using the ExPASy proteomics server (ca.expasy.org).

Sequences:

Silk: (His tag)-$[SGRGGLGGQGAGAAAAAGGAGQGGYGGLGSQGT]_{(6 \text{ or } 15)}$

A3: MSPHPHPRHHHT

R5: SSKKSGSYSGSKGSKRRIL

`

DNA vector digestion:

20µL of pet 30a vector with 6mer or 15mer silk sequence cloned into previously, 14µL dH_2O, 4µL buffer #2, and 2µL SpeI enzyme were mixed and incubated at 37°C for 1 hour. 10µL of Calf Intestinal alkaline Phosphatase (CIP) and buffer were prepared as follows: 9µL 10x buffer #3 was added to 1µL CIP enzyme. 5µL of the CIP mixture was added to the SpeI samples. After 30 minutes at 37°C, the other 5µL of the CIP mixture was added and again incubated for 30 minutes at 37°C to dephosphorylate the complementary SpeI ends and prevent vector from closing. To deactivate the CIP and SpeI enzymes, the samples were heat shocked for 10 minutes at 70°C. The samples were then run on a 1% agarose gel and stained with ethidium bromide with 6mer and 15mer uncut vectors. The samples of interest were visualized with UV light, cut out of the gel, and repurified.

DNA Extraction from Gel:

Gel extraction was performed according to the directions outlined in the Qiagen Gel Extraction Kit. Briefly, after the band was excised from the gel, 3 times the amount (w/v) of QG buffer was added (900µL) to the extracted portions. The samples were incubated at 50°C for about 10 minutes, periodically mixed by inverting, until the gel completely liquefied. 1 gel volume (300µL) of IPA was added to the sample and mixed. 750µL sample was applied to the spin column and centrifuged for 1 minute at 13,000 RPM. The flow through was discarded and the rest of the sample volume was applied to the spin column and centrifuged again. After discarding the flow through, 0.5mL buffer QG was added to the column, which was then centrifuged at 13,000 RPM for 1 minute. The flow through was discarded and 0.75mL buffer PE was added to the column, let stand for 5 minutes, and then was centrifuged at 13,000 RPM for 1 minute. The flow through was discarded and the sample was re-centrifuged with the same

`

conditions. 15uL elution buffer was then added to the spin column in an Eppendorf tube, let stand for 2 minutes, then centrifuged at 13,000 RPM for 1 minute. The samples were then frozen for later use.

B) Protein Expression

i) Transformation into RY Cells:

20µL *E. coli* RY cells were added to 2µL plasmid and left on ice for 20 minutes. The cells were then heat shocked at 42°C for 90 seconds and then returned to ice for 2 minutes. 80µL SOC media at room temperature was added to the sample, which was incubated at 37°C for 1 hour. The entire sample was plated on agar plates with LB and incubated overnight at 37°C.

ii) Protein Expression:

Test tubes were prepared with 5mL LB media, 5µL kanamycin, and 4 isolated colonies of RY cells from each plate for all 4 treatment groups. The samples were shaken at 37°C for 6-7 hours, at which time 250mL flasks were prepared with 50mL LB media, 50µL kanamycin, and 250µL culture that was just prepared and incubated. The new samples were shaken at 37°C overnight. 5mL culture from the overnight samples was added to 500mL LB media and 25µL/mL kanamycin in 2L conical flasks. The samples were shaken and incubated at 37°C until the optical density (measured by absorption) reached 0.6 at 600nm as compared to the LB media control. Once the optical density reached 0.6, 2.5mL of 100mM IPTG (0.5mM final concentration) was added and the cultures were shaken at 37°C for 4 more hours. The solution was then centrifuged at 10,000 RPM for 10 minutes and the liquid portion was discarded. The cells were weighed and 5 times that amount of lysing buffer B, in mL, was added. The cells were then resuspended by vortexing and centrifuged for 20 minutes at 10,000 RPM. The volume

`

of liquid was removed to a falcon flask, then divided by 4, and that much Ni-NTA resin was added to the samples. The flasks were shaken overnight to bind the proteins to the resin matrix.

iii) Protein purification:

Samples with Ni-NTA resin were poured into columns and let stand until all of the resin settled in the column. After collecting the flow-through, the column was washed 3 times each with buffers B, C, D, and E (using the same volume as resin added to the samples), collecting the liquid in a separate falcon tube each time. Buffers were composed of 100mM NaH_2PO_4, 10mM Tris-Cl, and 8M urea with a pH of 5, with the concentrations adjusted for the appropriate pH (B = pH 8.0, C = pH 6.3, D = pH 5.9, and E = pH 4.5).

Gel Analysis for Protein Purification:

Each collected sample from protein purification step was then run on a 4-12% Bis-Tris 15-well NuPAGE gel in MES SDS running buffer at 200V for 30 minutes. The gels were then fixed in fixing solution (50% v/v methanol plus 10% v/v acetic acid) for 10 minutes, which was then removed and Colloidal Blue staining solution was added (20% v/v methanol plus 20% v/v Stainer A). After 10 minutes, 5% v/v Stainer B was added and the gel was stained for 4-12 hours. The gels were then de-stained with water and photographed (using GeneSnap) and the pure samples were prepared for dialysis.

Dialysis:

Samples for dialysis were combined in 50mL falcon tubes. The protein pH was adjusted to 4.5. The dialysis solution, 20mM acetate buffer at pH 4.75, was prepared (0.6% v/v acetic acid plus 0.136% w/v sodium acetate). 15mer proteins were dialyzed using 2,000 MWCO cassettes while 6mer proteins were dialyzed using 100 MWCO membranes. Samples were dialyzed overnight, changing the buffer once later in the day. After dialysis with the acetate

`

(refolding) buffer, the solution was changed to dI H_2O, which was changed 3 times a day for 3 to 4 days.

Lyophilization:

Dialyzed samples were combined in 50mL falcon tubes and frozen in dry ice with 70% ethanol. Frozen samples were then lyophilized for several days to vacuum dry the protein samples.

C) Protein Film Preparation

Figure 6. Methods of casting and treating the silk films for characterization and cell study work

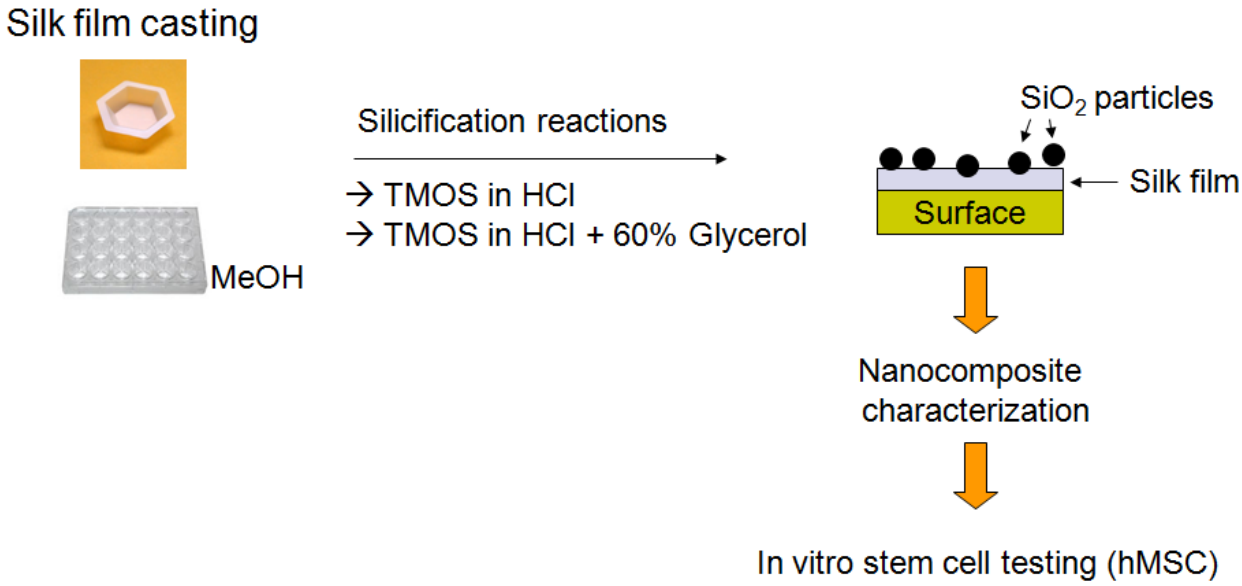

i) Protein film preparation:

Lyophilized samples were dissolved in HFIP (final concentration 2.5% w/v). Protein films were then cast and treated according to their experimental group. First, 50µL dissolved silk solution was cast on a plastic weigh boat to solidify for 3 hours. 1mL of 75% ethanol was added to the films and was left to dry overnight. 2mL phosphate buffer (pH 5.5) was then added to each film for 30 minutes. For each protein sequence, 3 films were made. 2 films were under normal silicification conditions and received 200µL silicic acid (tetramethylorthosilicate

`

(TMOS) pre-hydrolyzed in HCl). 1 film was treated with 60% glycerol (300µL glycerol plus 200µL TMOS). The films were left at room temperature for 1 hour. The films were then washed 3 times with water and allowed to air dry. After drying, the films were prepared and imaged using SEM (with Pt/Pd coating).

Part II: Cell Study

A) Protein Film Preparation

i) Protein Film Preparation:

Protein films were prepared as above (part I, section D), except 60µL dissolved silk/silica protein solution was cast on 24-well tissue culture plates instead of plastic weigh boats. Films cast on the tissue culture wells without silicification treatment were used as controls and were visualized using SEM imaging. All experimental films used in the cell study were treated with 60% glycerol and TMOS (as above) to promote silicification.

B) Cell Seeding:

i) Cell Seeding:

P2 bone marrow derived hMSCs were seeded on protein films in culture plate wells with a seeding density of 20,000 cells/well in 1mL MSC medium (440mL plain high glucose DMEM with L-glutamine, 5mL 1% non-essential amino acids (NEAAs), 5mL 1% pen-strep, 50mL 10% FBS, and 10µL bFGF). Cells seeded on the tissue culture plate (without protein films) were used as a control. The films were then photographed using light microscopy. After 2 days, the media was exchanged to remove any unattached or dead cells, and the films were re-imaged. Once the cells reached approximately 80% confluency, differentiation was induced (day 0) by changing to osteogenic media (425mL plain high glucose DMEM with L-glutamine, 5mL 1% NEAAs, 5mL 1% pen-strep, 50mL 10% FBS, 50µL 100nM dexamethasone, 10mL 10mM β-glycerol

`

phosphate, and 5mL 0.05mM ascorbic acid). Some cells seeded on the tissue culture plate without a film were not switched to osteogenic media (they remained in MSC media) and served as a negative control. Media was changed 3 times per week.

C) Cell Study Assays:

Cell culture assays (Alamar Blue assay, Pico Green assay, and qRT-PCR) were performed at 1 and 2 weeks after differentiation. The cells were imaged using light microscopy at the same time points as the assays were performed.

i) Cell Viability:

An Alamar Blue assay was used to determine the cell viability. The more metabolically active the cells are, the larger the difference in fluorescence of the assay solution as compared to the control. Briefly, media was aspirated from the wells and 500µL MSC media was added. 50µL Alamar Blue solution was added, the solution was mixed, and the cells were incubated for 2 hours at 37°C. 150µL of each sample containing the Alamar Blue solution was removed and pipetted into a separate well on a 96-well plate three times. The fluorescence of each sample on the plate was then read using SoftMax Pro software and compiled in a chart below (figure 14). 3 samples containing MSC media and Alamar Blue solution without cells was used as a standardized control fluorescence reading.

ii) Quantification of Double-Stranded DNA:

A PicoGreen assay was performed to quantify the double-stranded DNA present for each sample. Media was aspirated from the wells, which were then washed once with PBS. 1mL Working Solution B (10mL 1x TE buffer with 5µL Triton X-100) was added to each well. The cells were scraped from the well, pipetted in solution into Eppendorf tubes, and stored at 4°C. To quantify the amount of double-stranded DNA present, a fluorescent probe (reagent A, also

`

known as Quant-IT PicoGreen dsDNA reagent) was added to each sample as follows: 100µL working solution A (Solution B with 0.05% Reagent A) and 75µL 1x TE were added to 25µL sample, in triplicate. The fluorescence of each sample on the plate was then read using SoftMax Pro software and compiled in a chart below (figure 15).

iii) Gene Expression Quantification:

Gene expression was quantified using qRT-PCR. First, media was aspirated from the wells, which were then washed once with PBS. 0.35mL lysis buffer (1mL Qiagen Buffer RLT with 10µL mercaptoethanol) was added to each well being assayed. The cells were scraped from the well, pipetted in solution into Eppendorf tubes, and stored at -80°C.

mRNA was then isolated and purified on ice using an RNeasy Mini Kit (Qiagen). The samples were each added to QIAshredder columns and centrifuged at 13,000 RPM for 2 minutes at 4°C (all following centrifugations in this section were under these conditions unless otherwise noted). 350µL 70% ethanol was added to the eluent and the solution was transferred to an RNeasy column. The samples were then centrifuged again and the eluent was discarded. The sample was then washed with 700µL RW1 Buffer and 500µL Buffer RPE, centrifuging after each wash. The final wash was with another 500µL Buffer RPE, centrifuged for 4 minutes. 50µL RNAse-free water was added to each RNeasy column in new Eppendorf tubes and the samples were centrifuged a final time.

The samples were then reverse transcribed into cDNA using a High-Capacity cDNA Archive kit (ABI Biosystems). On ice, 5µL of RNA sample was added to 45µL RNAse-free water. 50µL RT master mix (containing 21µL DNAse free water, 10µL 10x RT buffer, 4µL 25x dNTPs, 10µL 10x random primers, and 5µL multiscribe) was added for a total volume of 100µL.

`

cDNA was synthesized in a thermocycler with the following program: 25°C for 10 minutes, 37°C for 120 minutes, and 4°C for 2-24 hours)

qRT-PCR was performed to measure the relative expression of specific osteogenic genetic markers as compared to GAPDH, a housekeeping gene. The genes of interest were alkaline phosphatase (ALP), collagen type I (ColI), and bone sialoprotein (BSP). An Assay-on-Demand kit was used to perform the reaction. Briefly, 5µL cDNA sample was added to 45µL master mix containing 17.5µL RNAse-free water, 25µL 2x TaqMan universal PCR kit, and 2.5µL Assay-on-Demand kit specific to each gene. The protocol was repeated for each gene of interest, including GAPDH, in triplicate. The thermocycler was run using a universal thermal profile setup with 50 repetitions. The resulting data was compiled and the expression of each gene was standardized with respect to the expression of GAPDH (figures 16-18).

iv) Imaging and Elemental Analysis of Scaffolds:

After completion of the cell study, remaining scaffolds were washed with DNase and RNase free water twice. The films were then allowed to dry overnight, and were prepared and imaged using SEM. To confirm the elemental composition of the samples, electron dispersal x-ray (EDAX) analysis was performed on the samples. The elements of particular interest for this study were calcium (Ca) and phosphorous (P) as they are found in hydroxyapatite ($Ca_{10}(PO_4)_6(OH)_2$) and calcium phosphate ($Ca_3(PO4)_2$), a hydroxyapatite precursor.

Part III: Statistical Analysis

Statistical analysis was performed on all measurements made using the various techniques listed above. A student's t-test was used to compare and assess differences in sample means. P-values less than 0.05 indicated statistical significance.

`

Results:

Precipitation of uniform silica particles on the surface of the chimeric protein films was successful, achieving our first and second specific aims. All films used in this study were treated with methanol to induce stable β-sheet secondary structure which provides mechanical strength for the studied materials. Films that did not undergo silicification reactions (e.g. no further chemical modifications after methanol treatment) were used as control samples (figure 7). For all samples that underwent silicification reactions, the precipitated silica was in the form of nanoparticles with average sizes of 200-400nm (see figure 8, below). The silicification reaction involved incubation of silk films in the TMOS solution pre-hydrolyzed in HCl with the addition of 60% (v/v) glycerol to the mixture to obtain low density of silica particles on the films. When 6A3 films were treated with TMOS only (no glycerol), the particles produced had a diameter of 421nm ± 121nm, but when they were treated with glycerol, they were 230nm ±107nm. Particles precipitated on 15R5 films treated with glycerol had a diameter of 378nm ± 100nm, which was larger than those from the 6A3 glycerol-treated films, but smaller than the untreated 6A3 films. Although the sample size was large in most cases (n ≈ 100), the particle diameters measured on each film were relatively evenly spread in a non-Gaussian distribution (data not shown) and therefore had high standard deviations and were not significantly different from one another.

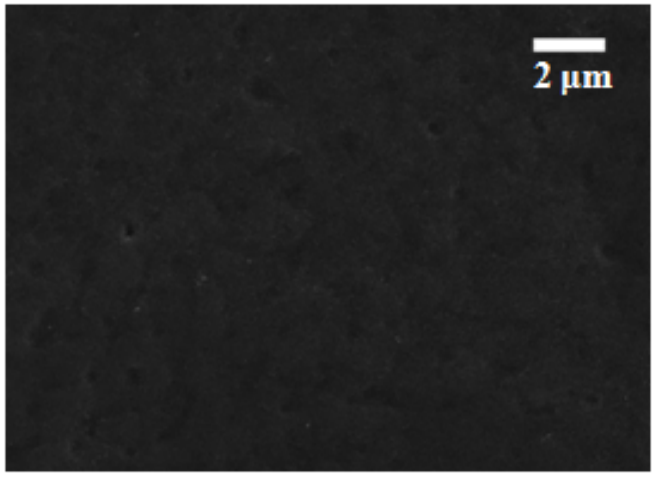

Figure 7 (left). 6mer film with no silicification reaction

`

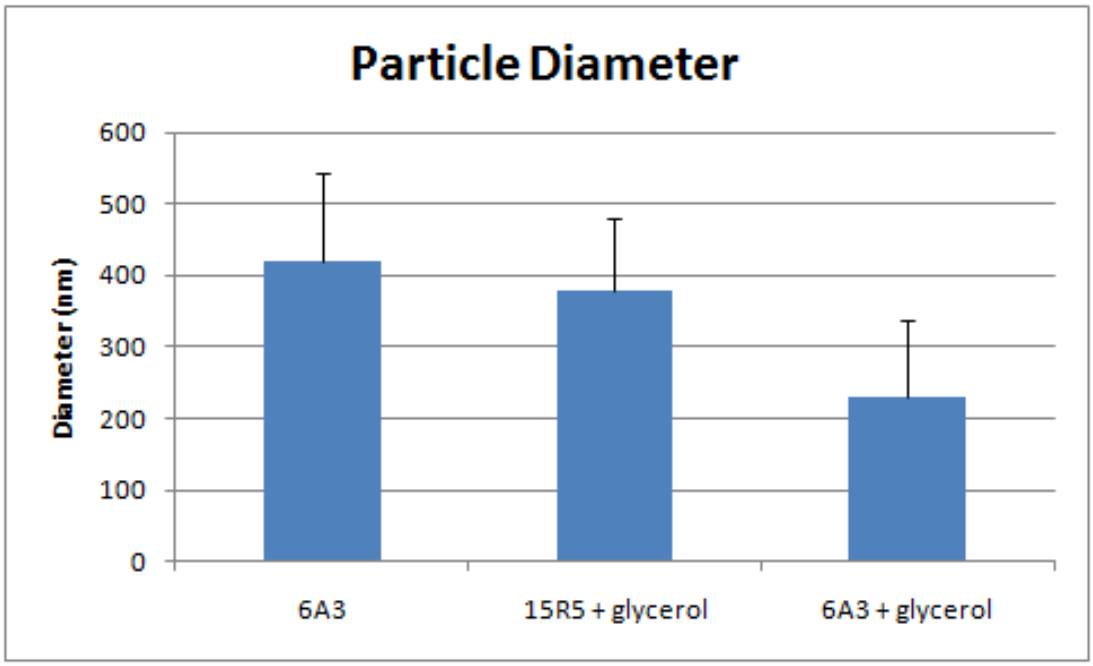

Figure 8. Particle diameter distribution on glycerol treated films

Although the morphology of particles precipitated on the silk films was similar, the glycerol treatment had profound effects on the positioning of the particles on the film surfaces (figure 9). Particles precipitated on surfaces that were only treated with TMOS were evenly distributed on the surface of the films, but tended to form clusters or groups of particles. These aggregated particles were much larger than individual particles that were precipitated on silk films treated with glycerol, a phenomenon that can be controlled synthetically (figure 10). See appendix A for additional images.

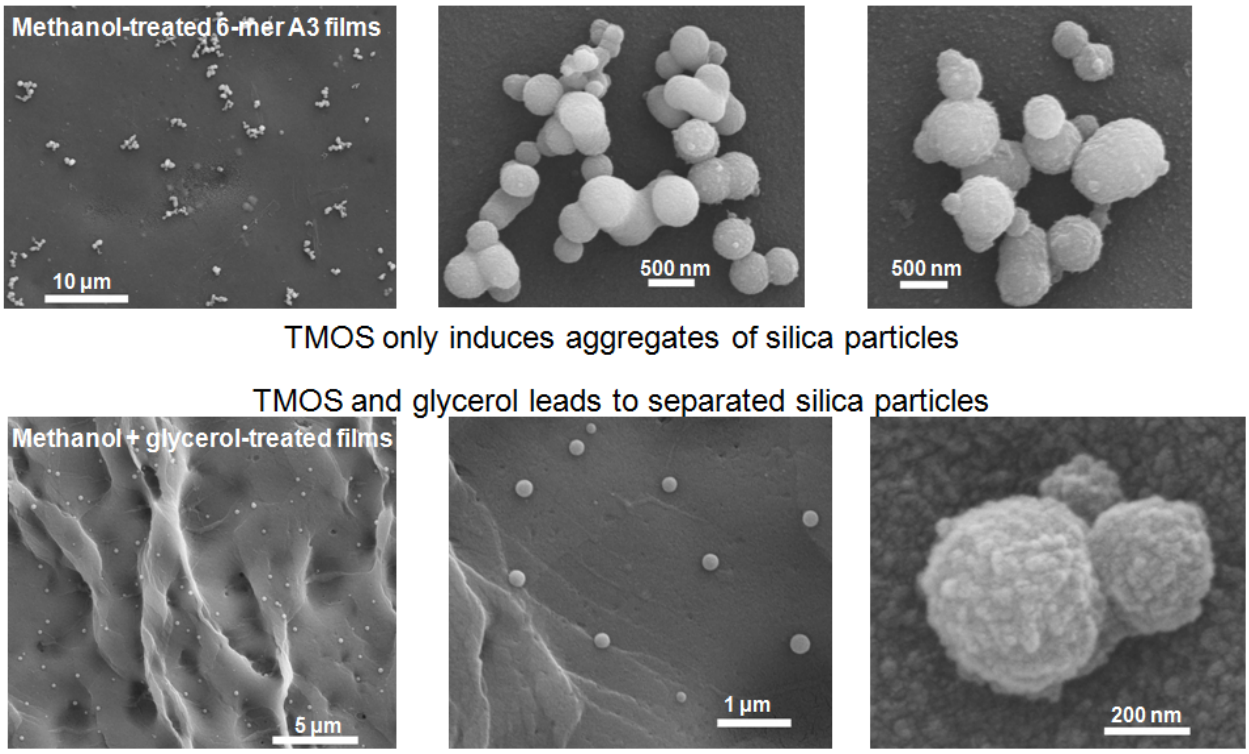

Figure 9. Methanol-treated vs. methanol + glycerol-treated 6A3 protein films demonstrate similar particle morphology but different distributions

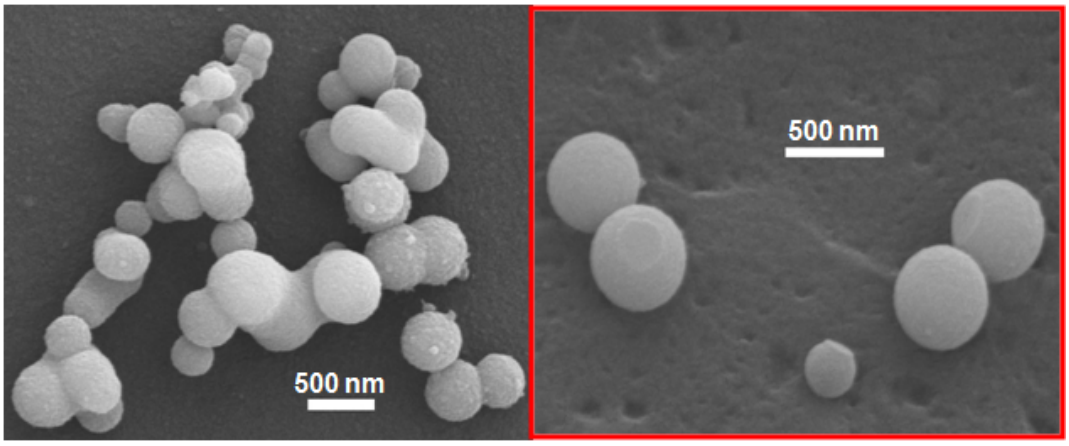

Figure 10. 6A3 films treated with TMOS (left) and TMOS + glycerol (right, red outline). Silica particles precipitated on the glycerol-treated films were spread out aggregated as compared to non-glycerol-treated films

`

Once successful precipitation of silica particles was achieved, before proceeding with the cell study portion, we had to confirm the successful precipitation of silica by protein films cast on tissue culture plates. We decided to study the osteogenic capabilities of cells seeded on films treated with glycerol with the intent of investigating non-glycerol treated films in a future study. The separation of silica nanoparticles on the silk films after TMOS/glycerol treatment offers potential for greater cell interactions with single particles. Due to the small size of the nanoparticles, the silica can also be integrated into the cell and further remodeled into bone-like material.

The silica particles which precipitated on the glycerol-treated films cast on tissue culture plates were comparable to those precipitated on glycerol-treated films used for material characterization (see figure 11). The particles were the same size and distribution, demonstrating spherical morphologies and individual, separated particles. The only difference was that the particles which precipitated on the weigh boat films had smooth surfaces, whereas those precipitated on the tissue culture plate had slightly irregular surfaces. However, the overall appearance of the particles on the TCP films was round so progression to cell seeding and cell assays was appropriate.

`

Figure 11. Differences in silica particles precipitated by 6A3 protein films on tissue culture plates and weigh boats were considered negligible as the particles were of the same size and distribution

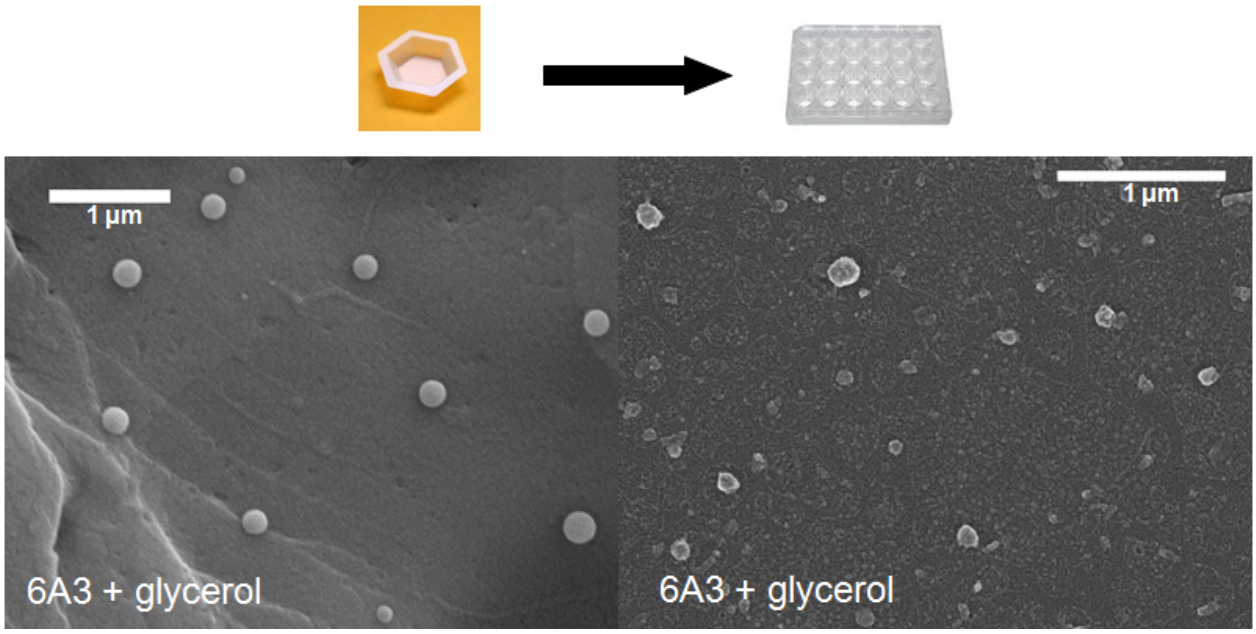

hMSCs were successfully seeded on chimeric protein films cast on tissue culture plates (TCPs). Silk films without silicification as well as TCP only were used as controls. On the day of cell seeding, the cells were small and demonstrated a round morphology, as expected. After 2 days in MSC media, the cells attached to the film or TCP, as evidenced by a more elongated morphology. Once the cells reached 70-80% confluence (d0 osteodifferentiation), they were changed to osteogenic media. Some cells seeded on the TCP remained in MSC media as a negative control. After 1 week, the cells were significantly elongated and formed large clusters or even sheets of cells on the surface of the protein film. The cells were often similarly oriented, demonstrating organization and communication between the cells, as shown in figure 12. The

`

cells at week two looked very similar to those at week one. Additional images of the cells on different films and surfaces at all time points can be seen in appendix A.

Cells seeded directly on the TCP in both types of media proliferated greatly (figure 13). The cells completely covered the surface of the TCP wells. After two weeks of culturing, cells seeded on the TCP in MSC media (negative control) were somewhat elongated and were oriented in a similar direction. Cells seeded on the TCP in osteogenic media were more elongated, evidence that they differentiated, and began to form cluster-like masses, but to a lesser extent than cells seeded on the silk films. The clustering of cells on the surfaces was most frequent on the chimeric protein surfaces, then on silk-only surfaces, then on TCP in osteogenic medium, and least frequent on TCP in MSC medium, as shown in figure 13. Additional images of the cells can be seen in appendix B.

`

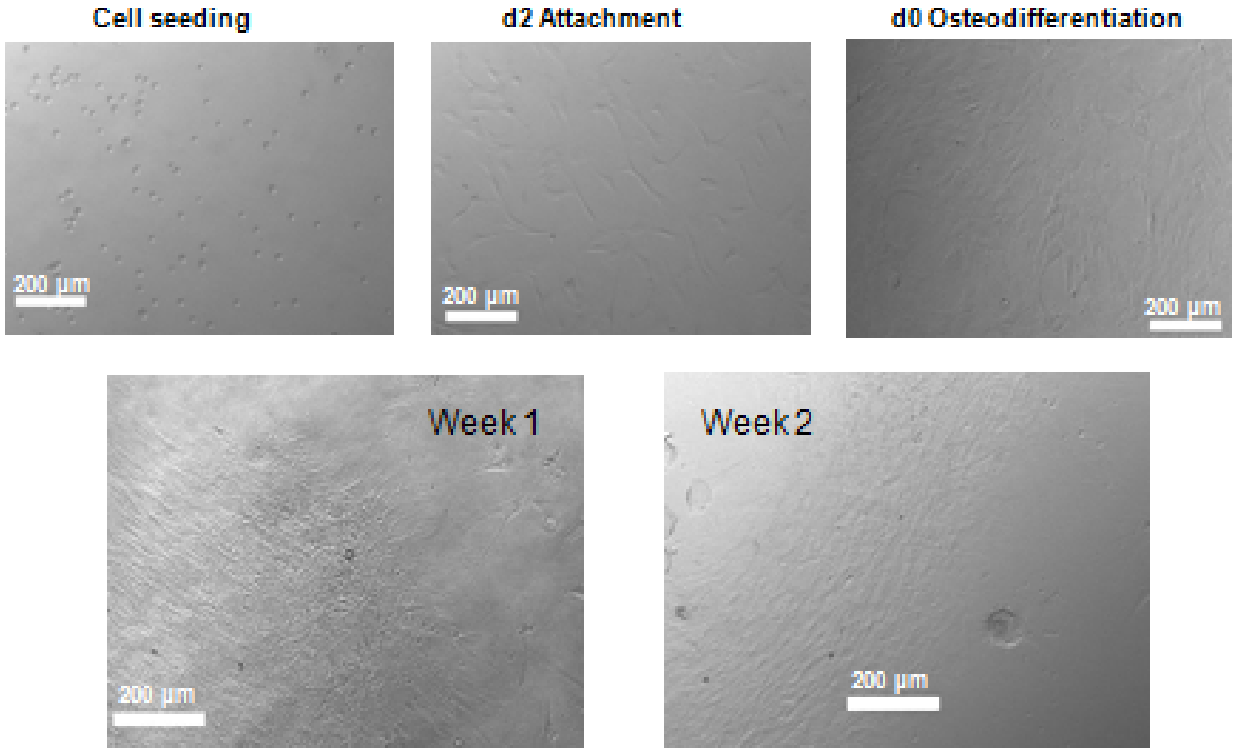

Figure 12. Cell proliferation and differentiation on 6R5 silk/silica protein films after seeding cells, attachment after 2 days, after changing media from MSC media to osteogenic media, and for week 1 and week 2 assays

`

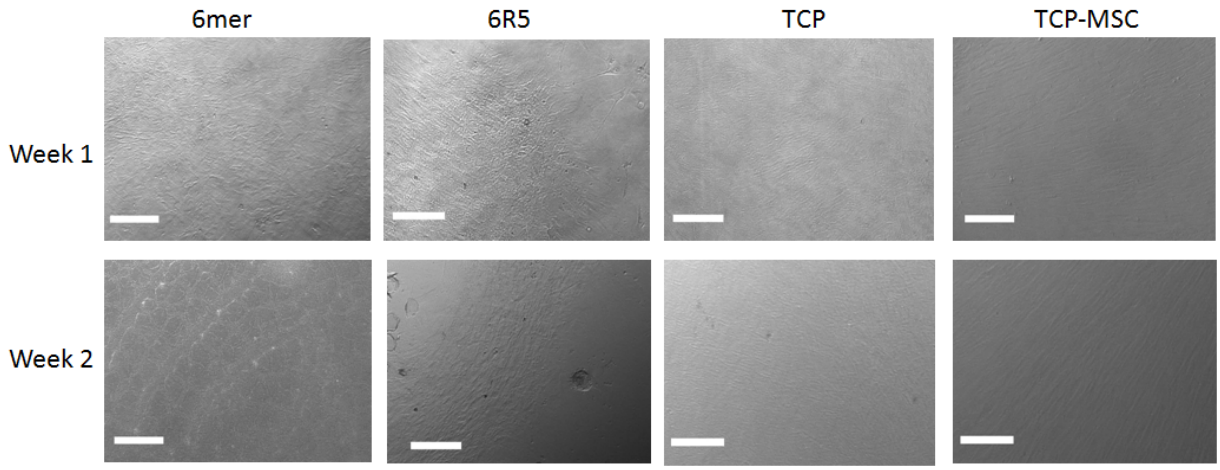

Figure 13. Light microscopy images of cells at week 1 and week 2 assay time points in osteogenic media on 6mer or 6R5 films or directly on TCP. Cells on TCP with MSC media only (on right) were the negative control.

Alamar Blue and PicoGreen assays confirmed that the cells on the protein films (and TCPs) were viable at both assay time points (week 1 and week 2), as shown in figures 14 and 15. All samples exhibited metabolic activity as measured by the detected fluorescence of the Alamar Blue reagent after 2 hour incubation at 37°C. Alamar Blue results from cells on both the 6A3 and 15mer protein films were significantly different between week 1 and week 2 with week 2 values being lower than week 1, but the cells were still viable. PicoGreen results confirmed the viability of cells as double-stranded DNA (dsDNA) content was quantifiable and was around 20-40 ng/mL for all samples at week 2. These differences were statistically significant ($p < 0.05$) from the TCP cells except for the 15mer sample. Samples were compared with a student's t-test and measurements were taken in triplicate. Samples from week 1 had dsDNA contents around 20 ng/mL, but due to limited availability of testing wells, only the 6mer and 6A3 films were assessed with the PicoGreen assay at this time point.

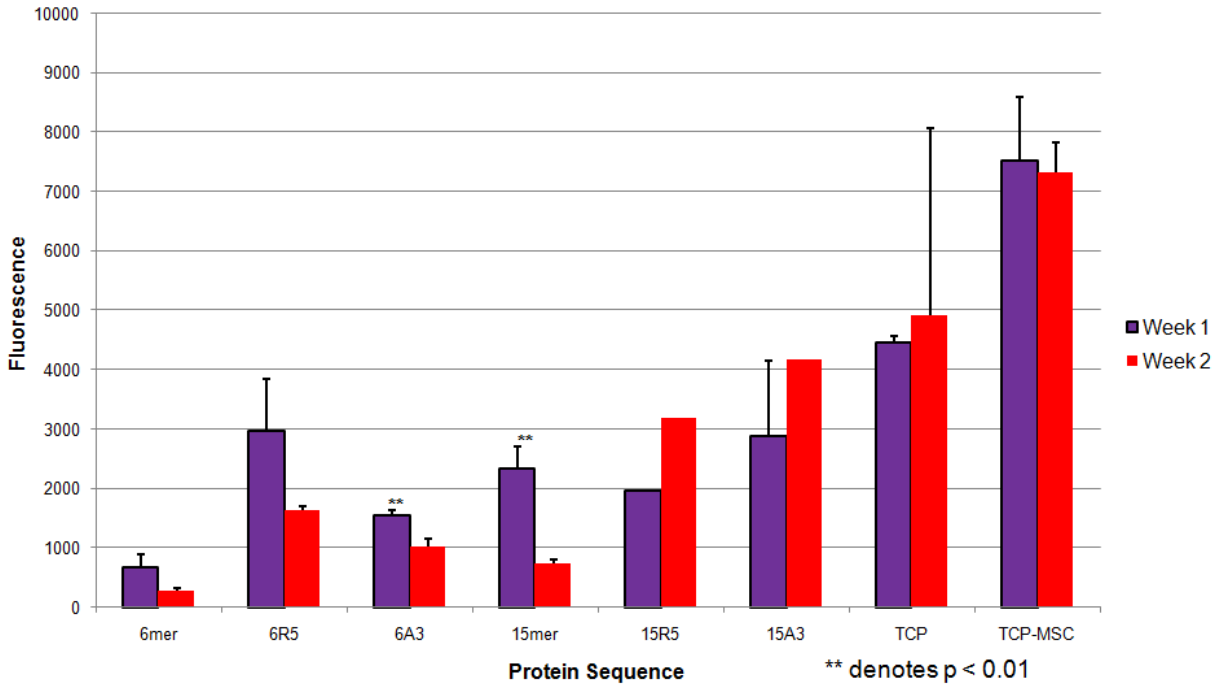

Figure 14. Alamar Blue cell viability assay results at week 1 and week 2 time points

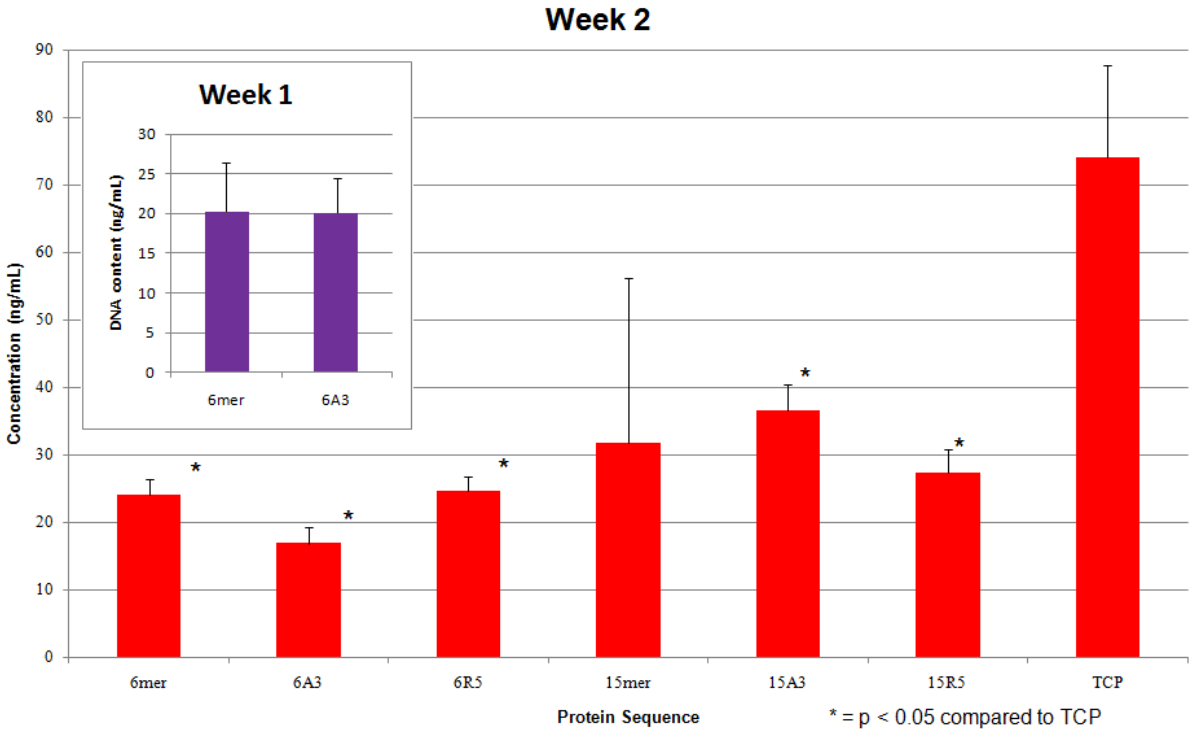

Figure 15. PicoGreen dsDNA content assay results

`

Gene expression was assessed using quantitative RT-PCR methods. (Note: indicators of statistical significance for all gene expression assays are as follows: * = $p < 0.05$ compared to TCP, ** = $p < 0.01$ compared to TCP, § = $p < 0.05$ compared to TCP-MSC, and §§ = $p < 0.01$ compared to TCP-MSC). The results were similar between the week 1 and 2 assays, and demonstrated osteoinductive properties on the chimeric protein films, achieving specific aim 3.

ALP was upregulated at both time points (figure 16), and expression was higher in 15mer and 15R5 samples as compared to the TCP with MSC media samples ($p < 0.05$ and $p < 0.01$, respectively) at week 1. At week 2, 6R5 and 15R5 samples expressed ALP more than samples on the TCP with osteogenic and MSC media ($p < 0.01$).

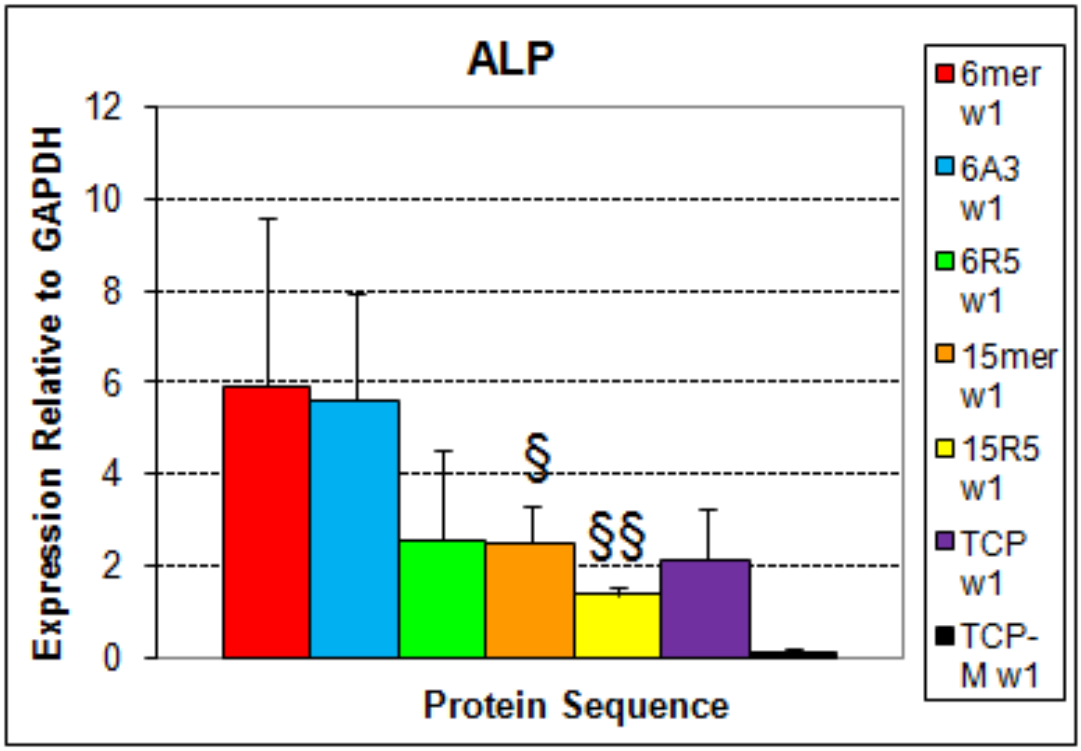

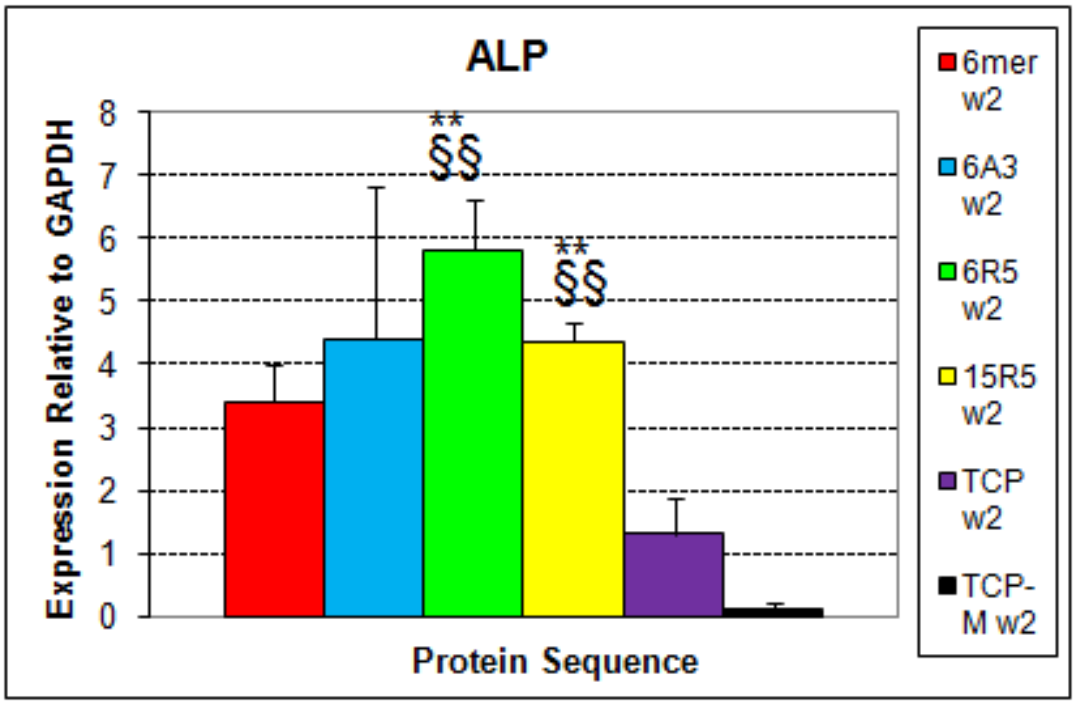

Figure 16. ALP expression at weeks 1 (top) and 2 (bottom)

`

The overall trend for BSP expression was upregulation from week 1 to week 2 (figure 17). The BSP expression of 15A3 samples at the week 1 time point were different from the other samples. All samples demonstrated similar increased levels of BSP expression, which indicates the occurrence of increased mineralization and osteogenic properties.

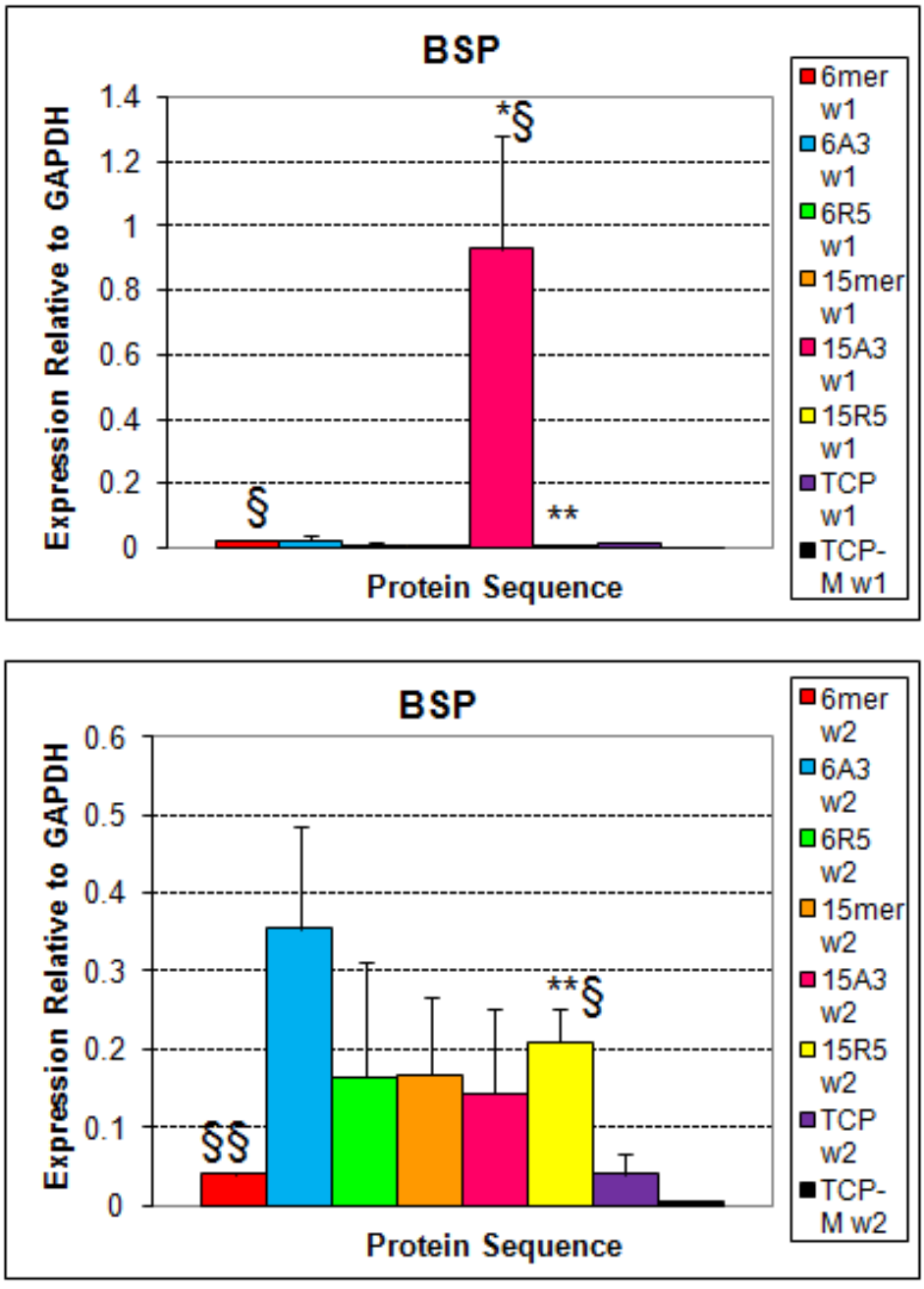

Figure 17. BSP expression at weeks 1 (top) and 2 (bottom)

`

Collagen type I expression was downregulated from week 1 to week 2, which was an unexpected result (figure 18). At the week 2 time point, all experimental samples demonstrated statistically significantly lower collagen type I expression as compared to the controls. Additionally, the collagen type I expression of the experimental samples was lower at week 2 than at week 1, suggesting that collagen was downregulated at week 2. All of the gene expression results combined, especially the ALP expression, confirmed our hypothesis that different protein sequence combinations would produce varied osteogenic properties.

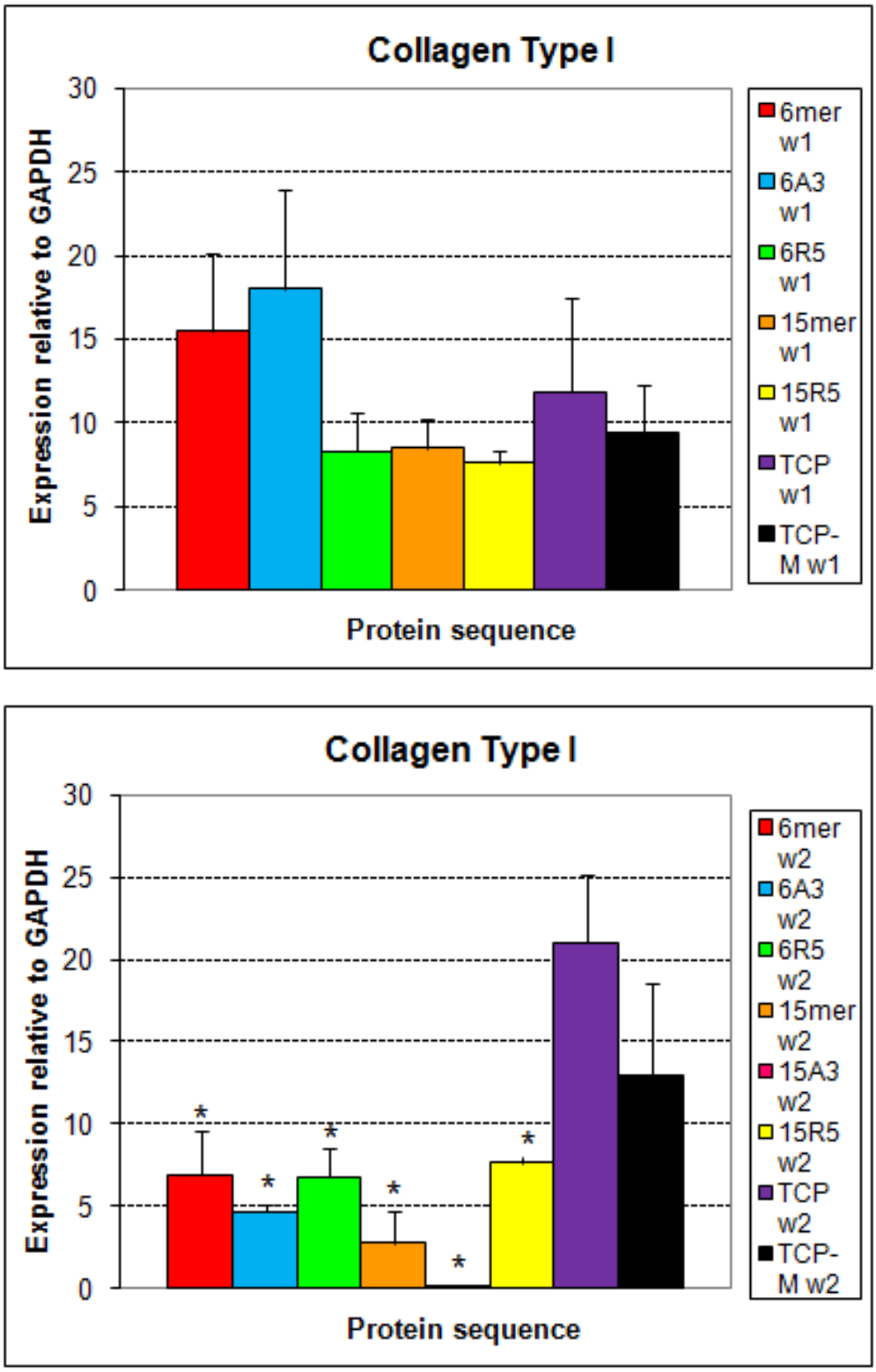

Figure 18. Collagen type I expression at weeks 1 (top) and 2 (bottom).

`

After completion of the cell study, the morphology and chemical composition of the films were analyzed using SEM imaging and EDAX techniques. The SEM images confirmed the morphology of the particles and extent of mineralization after 2 weeks of cell culture. EDAX analysis confirmed the elemental composition of the films, with particular interest in the presence of calcium deposition.

The EDAX (figure 19) and SEM (figure 20) results confirmed that biomineralization had occurred to differing degrees on the protein films; all films demonstrated at least a little bit of calcium phosphate deposition (figure 21). The TCP had the lowest amount of calcium phosphate mineralization with 0.21 atomic percent of calcium. The mineralized deposition was indistinct, globular, smooth, and not well developed. The 6mer film showed a little more calcium deposition, with 1.78 atomic percent of calcium, widely distributed throughout the field of view. The deposited material was still rounded and smooth as well. Adding the silica sequence, in this case the R5 sequence, increased the calcium content to 8.88 atomic percent, demonstrating biomineralization both on the surface of the silica particles and on the surface of the film. The deposited material was irregular and had needle-shaped protrusions, which is characteristic of the middle stage of hydroxyapatite (toward spherical crystals), where calcium phosphate had been deposited and was more mineralized than the amorphous (polymorphous) stage. Additional EDAX spectra and analysis can be seen in appendix C.

Figure 19. Elemental analysis of chimeric protein films after 2-week cell study

Surface	EDAX Spectrum	Atomic Composition
6mer	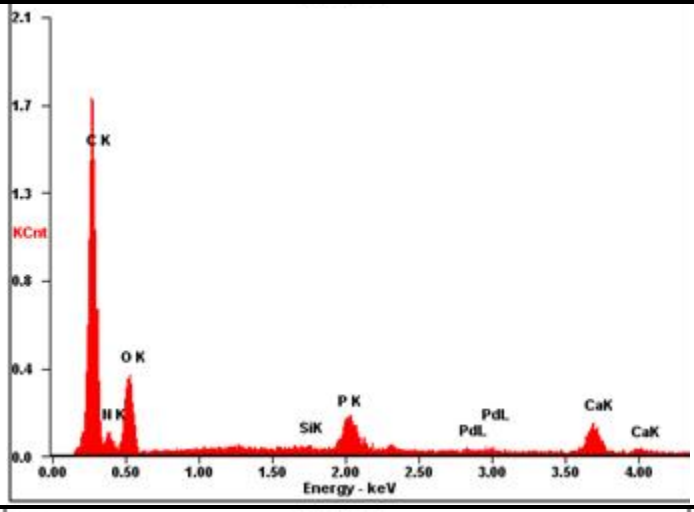	
6R5	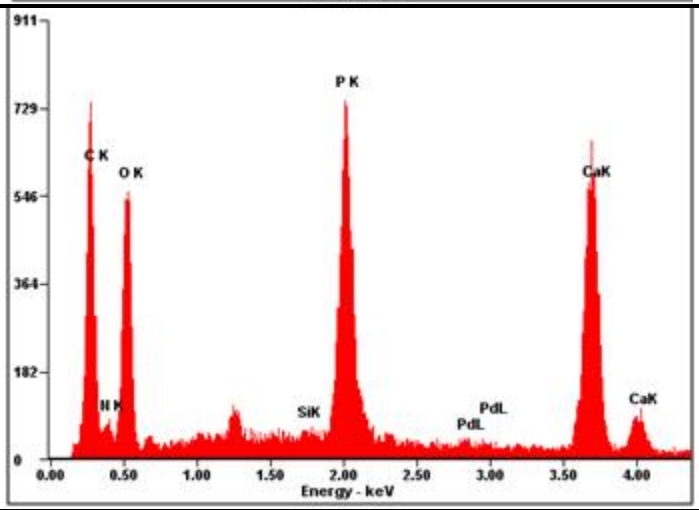	
TCP	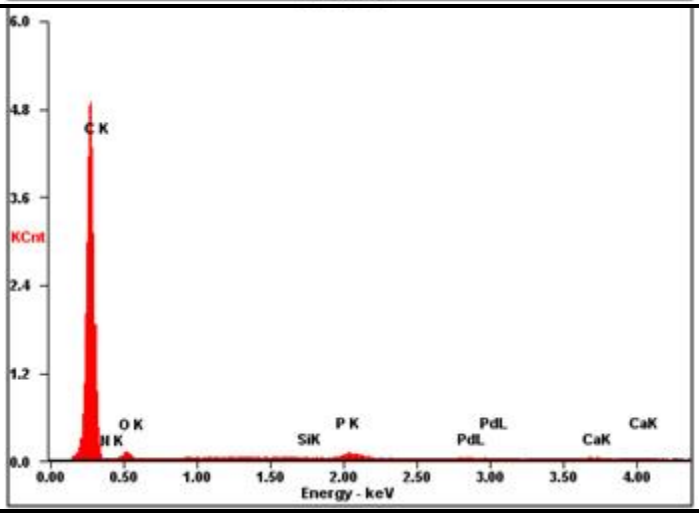	

Element	Wt %	At %
C K	47.38	63.85
N K	11.40	13.18
O K	18.06	18.27
Si K	00.18	00.11
P K	02.78	01.45
Pd L	00.80	00.12
Ca K	04.40	01.78
Pt L	15.00	01.24

Element	Wt %	At %
C K	25.36	42.60
N K	07.21	10.38
O K	23.76	29.97
Si K	00.12	00.09
P K	09.70	06.32
Pd L	00.99	00.19
Ca K	17.64	08.88
Pt L	15.21	01.57

Element	Wt %	At %
C K	82.10	94.13
N K	01.03	01.01
O K	03.95	03.40
Si K	00.00	00.00
P K	00.86	00.38
Pd L	00.96	00.12
Ca K	00.62	00.21
Pt L	10.49	00.74

`

Figure 20. SEM images of TCP (left), 6mer protein film (center), and 6R5 protein film (right) after 2-week cell study

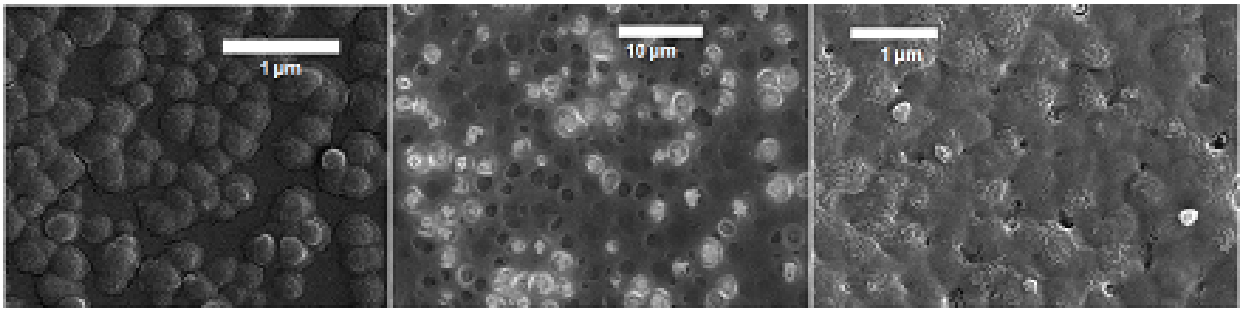

Silk films from the cell study were analyzed with EDAX techniques with a field of view around 200x200µm which was large enough to be considered a representative sample of the film. The main elements of interest were calcium, phosphorous, and oxygen, the main moiety present in hydroxyapatite and its precursor, calcium phosphate. Since the platinum peak (from the sample sputtering) was very close to the phosphorous peak, it was possible that their signals overlapped, and therefore it was difficult to determine how much of the phosphorous peak was attributable to phosphorous alone. We chose to quantify the mineralization capabilities by the calcium content because calcium should not be present on the films unless biomineralization has occurred (figure 21).

`

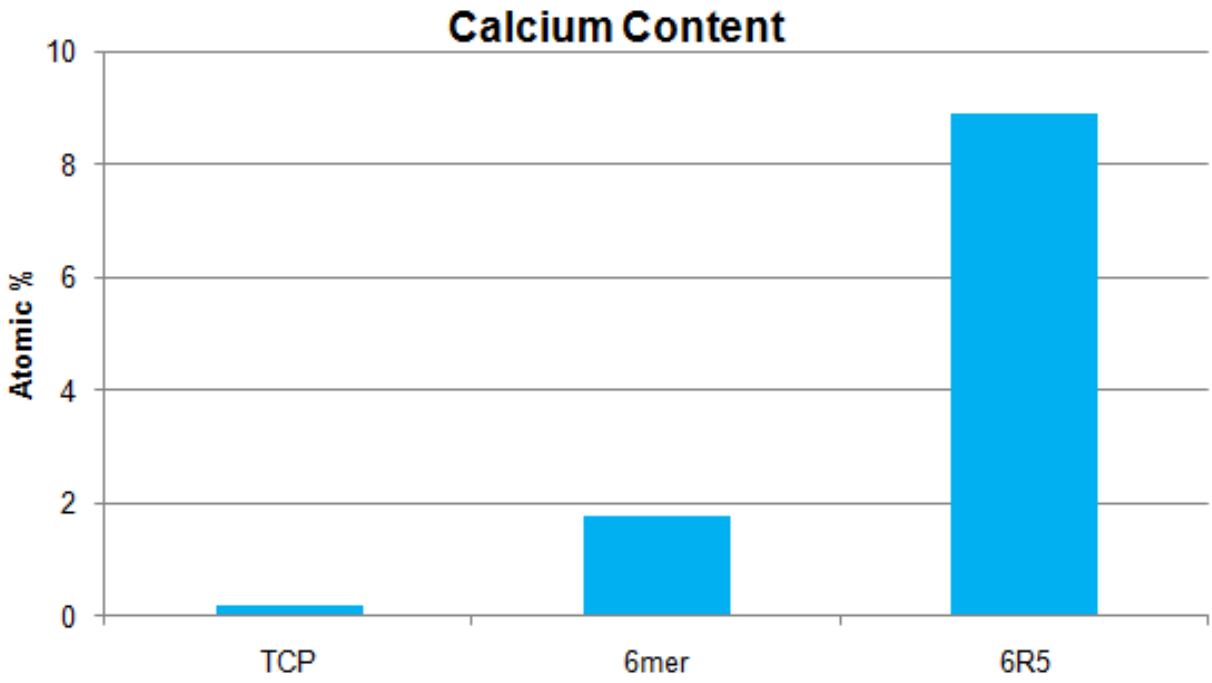

Figure 21. Calcium content increased on protein films and was enhanced by the insertion of a silica sequence in the chimeric protein

`

Discussion:

We successfully engineered and produced chimeric protein films with different precipitated morphologies and distributions which supported osteogenic activities of hMSCs, confirming our hypothesis. We achieved all of our specific aims by producing, characterizing, and successfully differentiating hMSCs on our protein films. Although some of the gene expression results were inconclusive, these preliminary results suggest that these proteins can be used in future studies toward dentinogenic restoration *in vivo*.

The results of the silicification reactions successfully demonstrated the ability to control silica morphology on the surface of the silk films (figure 22). The silica precipitation mechanism is based on electrostatic interactions between negatively charged silicic acid monomers and positively charged silica precipitating oligonucleotides embedded in the silk film. When the films were treated with methanol followed by TMOS only, the particles precipitated in aggregated groups as a result of full exposure of positively charged amine groups of R5 and A3 oligonucleotides. Although each individual particle still had a diameter of 200-400nm, the aggregates were much bigger than that, and therefore were too large for the cell to take up the particles. Therefore, we believe that the cells could still use the silica particles for attachment and to promote osteogenesis, but could not use the particle for remodeling.

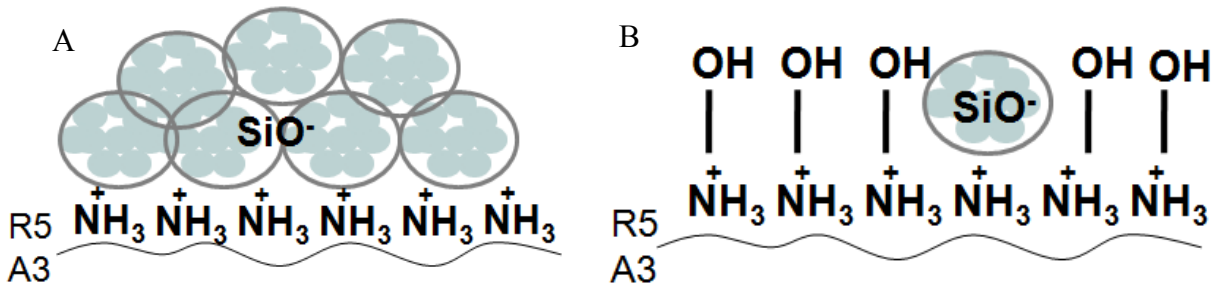

Figure 22. Proposed silica precipitation mechanism when silk films were treated with TMOS only (A) or TMOS + 60% glycerol (B).

`

Particle diameter results may suggest that the increased organic load of the 15mer protein films as compared with the 6mer protein films may precipitate slightly larger particles. Additionally, glycerol may affect the particle size as well; the mean for glycerol treated particles on various silk/silica sequence protein films were less than those from untreated films (230nm ±107nm and 378nm ± 100nm versus 421nm ± 121nm).

The films treated with glycerol demonstrated individual, separated silica particle morphology. We believe that induced hydrogen bonding between hydroxyl groups of glycerol and the positively charged amine groups of the silica sequences effectively blocked R5 and A3 molecules from precipitating silica. Therefore, the TMOS was only able to interact with a limited number of positively charged silica precipitating sites, producing individual particles that could be used for cell attachment and osteoinduction, in addition to bone remodeling.

Differences in surface morphology between films cast on the weigh boats for material characterization and on the tissue culture plates for stem cell studies were observed but were considered to be negligible. Although the size and distribution of the silica particles were the same, particles precipitated on the weigh boat were round and demonstrated very regular, smooth surfaces, while those precipitated on the tissue culture plates had irregular surfaces. This may be accounted for by the fact that the silk films could be peeled off of the weigh boats for characterization, whereas the films cast on the tissue culture plates could not. The stronger association between the silk and the tissue culture plate, perhaps due to electrostatic interactions, may have contributed to these observed differences. Although the particles demonstrated different surface morphologies, the particles were still similar to those precipitated on the weigh boats so advancement to cell studies was appropriate.

`

Cells seeding and differentiation was successful on the protein films as the cells attached to the surface and demonstrated osteoblast-like characteristics after changing to differentiation media at 70-80% confluence. Differentiated cells showed elongated morphologies and tended to be found in clusters or sheets of cells. These results suggest that the cells could be induced to differentiate by changing the media. Clustering of cells is a good result because it increases communication between cells and can allow them to better promote osteogenesis. Although most films demonstrated sheet-like covering of the film surface, the cells were sometimes difficult to discern from the film using light microscopy. This may be due to the fact that the cells could have completely covered the film in close proximity to one another. Cells at weeks one and two had similar morphologies, which may be due to the short duration of cell culture time and they may have more pronounced morphologies at a later date, which could be a direction for future work.

The cells from all experimental groups were viable. The cells on the TCPs and TCPs with MSC media demonstrated the highest Alamar Blue results, which was likely due to an increased number of cells present on the surface of the TCP (cells tend to stick and proliferate well on the TCP surface), as evidenced in figure 13. We did not expect the dsDNA content to be so much lower in the experimental groups than on the TCP, so this is an area warranting further investigation.

Overall, the gene expression results were inconclusive and the outcomes should be confirmed. Generally, the expression of the 3 genes of interest, ALP, BSP, and ColI, were relatively similar between week 1 and week 2 suggesting that there was no appreciable difference between the genetic expression of the cells at these time points. This may be due to the fact that the cell study was short, so latent differences may become apparent or more

`

pronounced if a cell study was conducted over the period of 4-8 weeks. Additionally, these gene markers are present to differing degrees depending on the length of culture time – if the cell study had encompassed more time points, most likely the ALP expression would have eventually decreased as ALP is an early osteogenic marker that is not highly expressed after 4-6 weeks.

The specific results from the gene expression analysis should be critically assessed and demonstrate preliminary results that can be used as a comparison for future studies but should not represent definitive results. Expression of all 3 genes of interest were similar between weeks, although ALP was significantly upregulated in the 6R5 and 15R5 samples at week 2, suggesting that the R5 sequence may contribute to the upregulation of ALP expression more so than the other silica sequences. The 15A3 BSP expression was markedly different between weeks, which may have been a fluke, as suggested by the large mean and standard deviation at the week 1 time point, especially compared to other samples measured that week. Repeated analysis of this sample should be performed.

The collagen type I expression results were unexpectedly low as compared to the controls. We would have expected to see a continued increase in collagen type I expression as the ECM deposition should be upregulated as osteogenesis occurs and collagen type I is a major organic component of the ECM. Since ALP was upregulated, the cells appear to be promoted toward osteogenesis, but it is unclear to what degree.

These results of the EDAX analysis suggest that the silica sequences are important for encouraging mineralization as calcium content was greatly increased for the 6R5 film than the 6mer film. However, there were conflicting results with the 15mer film since it demonstrated much higher calcium content than the 15R5 film (10.57 and 4.08 atomic percent, respectively). The 6A3 film had a similar result, having 0.78 atomic percent calcium compared to 1.78 atomic

`

percent on the 6mer film. The variance in these results may arise from the small number of films that were analyzed (one per silk/silica sequence due to limited materials and time). Additionally, the fact that the 15mer film with no silica sequence precipitated so much calcium phosphate is of interest because it may demonstrate that the organic load of the protein is important for biomineralization. These results suggest that the silica and silk sequences may be important to promote mineralization, but further investigation is warranted with a higher replication of samples and perhaps a longer duration of culturing cells to further distinguish the mineralization capabilities of each protein film.

The calcium content and shape of the mineralized particles on each film demonstrate the degree to which the cells deposited mineralized hydroxyapatite. A characterization of particle shapes and distributions was previously established (Gajjeraman, et al., 2007) to illustrate a continuum of development from depositing calcium phosphate (initial stages) to hydroxyapatite (complete mineralization). The development of hydroxyapatite formation was characterized by several stages, where the initial stage of mineral deposition is in the form of calcium phosphate, $Ca_3(PO_4)_2$, which eventually progresses through morphological changes toward hydroxyapatite, $Ca_{10}(PO_4)_6(OH)_2$. Although they used different methodologies of precipitating silica over a longer period of time, the developmental trend is clear and can be easily identified morphologically (figure 23). The initial calcium phosphate deposition demonstrates coiled, spherical structures and is relatively amorphous. The middle stage of development is characterized by the controlled production of needle-shaped crystals. The crystals are not yet hydroxyapatite but they do have definitive shapes. The final stage, hydroxyapatite formation, is characterized by spherical lobes of nanocrystals that have needle-like protrusions covering the surface of the particles. The number of needles and width of the particles increases as the

`

crystallinity increases and hydroxyapatite is formed. In the study mentioned, the crystals increased to nearly 30 µm in diameter after 7 weeks and were completely covered in needle-like spikes.

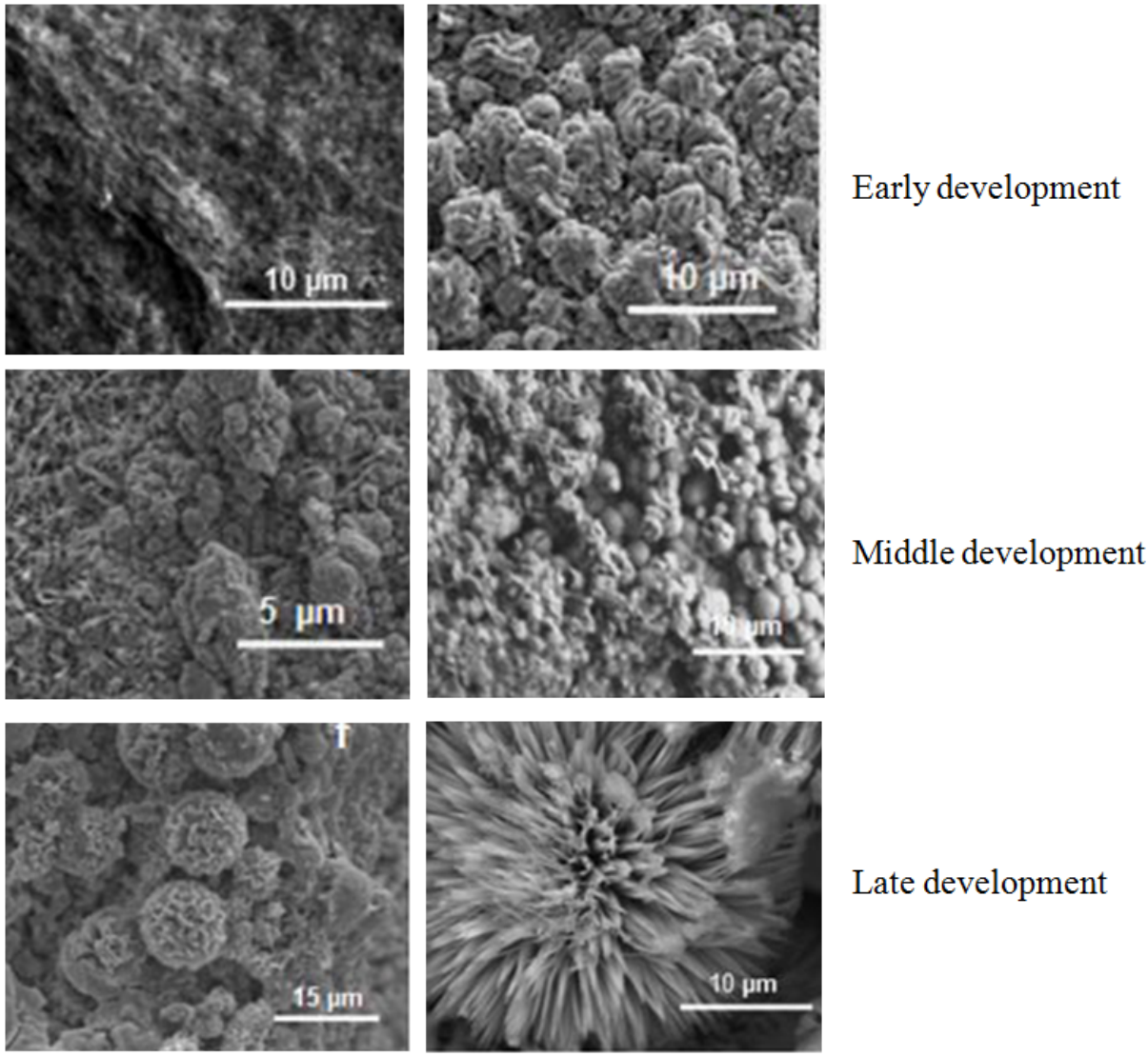

Figure 23. Development of biomineralization deposits from amorphous calcium phosphate to controlled, regular, spherical hydroxyapatite crystals (Gajjeraman et al., 2007)

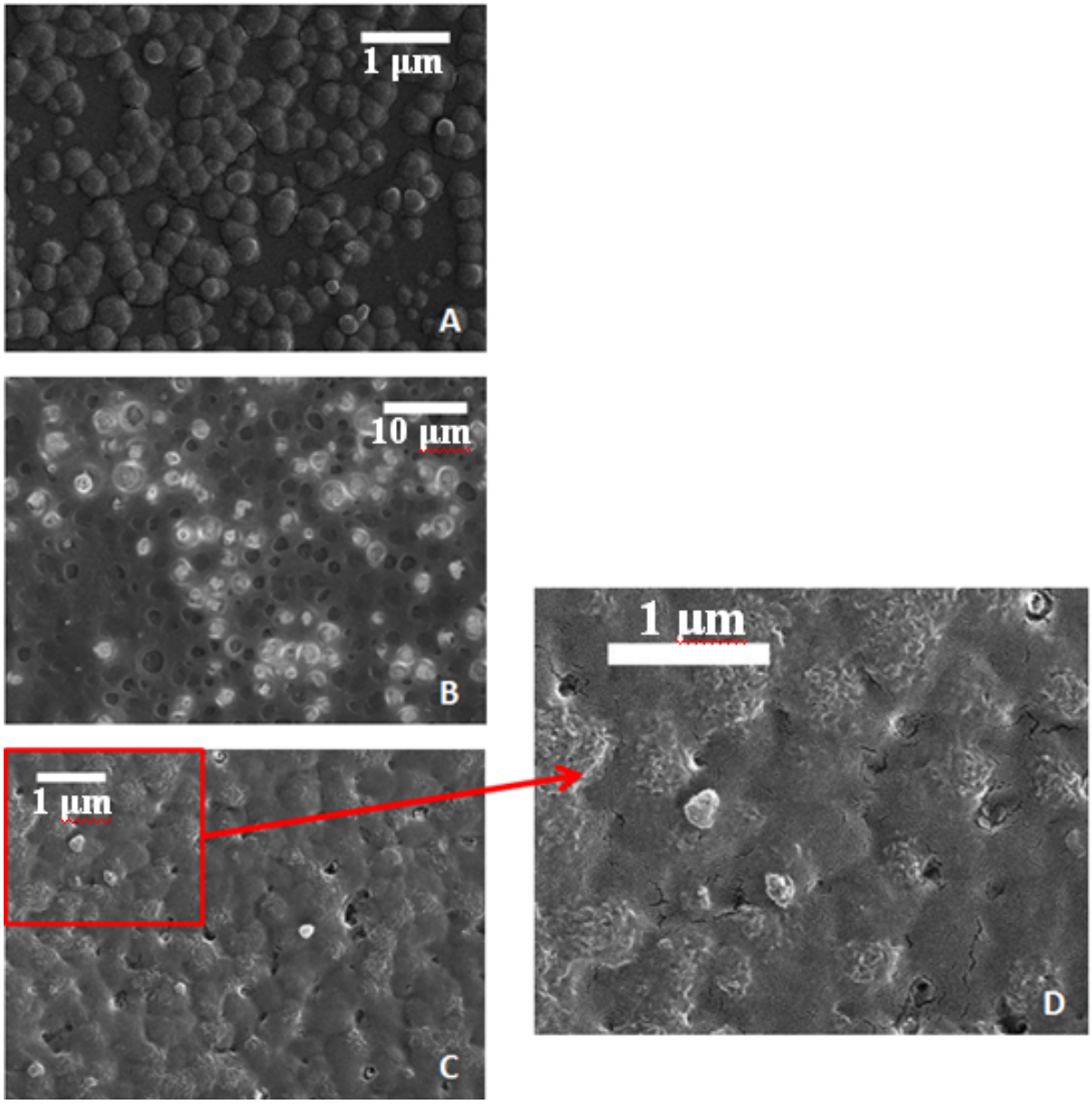

Figure 24. Development of biomineralization deposits on (A) TCP with osteogenic medium [early development], (B) 6mer silk film [early-middle development], and (C) 6A3 chimeric protein film [middle development]. (D) is an enlarged image demonstrating the development of needle-like spikes

`

The surface with the lowest calcium content, the TCP, was the least developed on the progression of hydroxyapatite mineralization, which was also evidenced by the round, smooth deposition of calcium phosphate on the surface of the tissue culture plate (figures 20 and 24). The 6mer film showed further development toward hydroxyapatite formation than the TCP, but less than the 6A3 film. The 6A3 film surface was further developed towards hydroxyapatite formation, demonstrating needle-like protrusions and a higher calcium content. Development of hydroxyapatite formation was characterized based on morphology, as compared between figures 23 and 24. A longer cell study (4-8 weeks) would be necessary to better assess complete formation of hydroxyapatite crystals on the chimeric protein films.

`

Conclusions:

Our preliminary results demonstrate that silk/silica nanocomposites can be formed through a genetic engineering approach. The silica particle size and distribution can be reproducibly controlled synthetically by varying the silk and silica sequences of desired proteins and applying various chemical treatments. Regular, spherical particles on the order of 200-400nm were successfully precipitated, which tended to form individually after undergoing silicification reactions with glycerol but particles aggregated when silicification reactions did not contain glycerol. These results translated well to casting films on TCPs as well.

hMSCs successfully attached well and were viable on the protein film surfaces, as confirmed by Alamar Blue and PicoGreen assays. The cells differentiated and deposited calcium phosphate on the surface of the films and silica particles in a 2-week cell study, but the quantitative RT-PCR results were inconclusive as to the extent of osteogenic capabilities of the cells on the scaffolds. SEM imaging and EDAX analysis confirmed the deposition of calcium phosphate on the surface of the films and silica particles, which is an initial step toward hydroxyapatite formation and osteoinduction.

`

Future Work:

Future work would certainly require repetition of the experiments to confirm these preliminary results. This would include an investigation of the osteogenic capabilities of cells seeded on protein films that underwent silicification reactions without the addition of glycerol. Silica precipitating sequence content of the chimeric proteins could also be investigated to determine an ideal concentration of precipitated silica particles on the surface of the protein films. Alternatively, other silica sequences, in lieu of A3 and R5 sequences, could be inserted and their osteoinductive properties could be assessed using the same procedure. A longer *in vitro* cell culture time (4-8 weeks) would provide additional insight into the mineral deposition and gene expression of cells seeded on these scaffolds as a function of time, and supplementary genes of interest for osteogenesis could include osteopontin and osteocalcin expression.

In the long term, a movement toward 3-D chimeric protein scaffolds would provide additional knowledge that would be applicable in a clinical setting. These studies should include degradability analysis, as assessed by histology and confocal imaging techniques. Finally, movement toward *in vivo* studies in mice is encouraged as a step toward eventual implantation in humans to promote dentinogenic restoration after tooth injury or decay.

`

Appendix A: Scanning Electron Microscopy Images

Appendix A1. Representative Images for Material Characterization

6A3 Regular	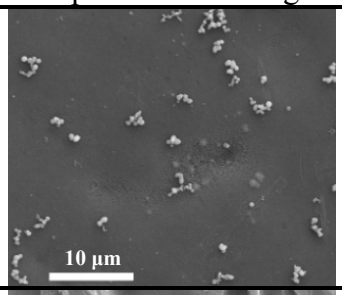	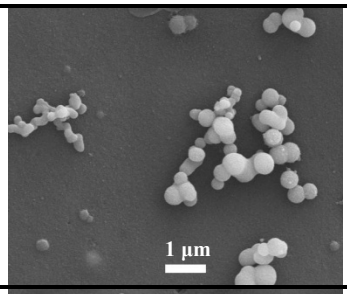	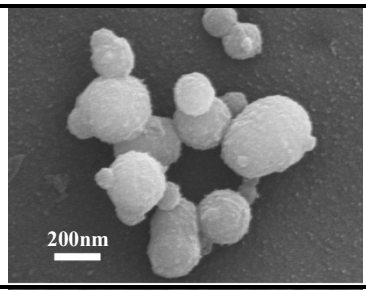
6A3 Glycerol	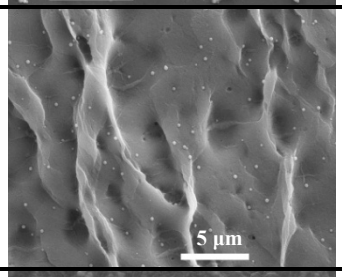	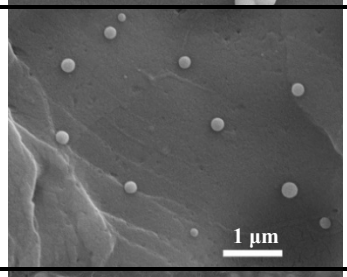	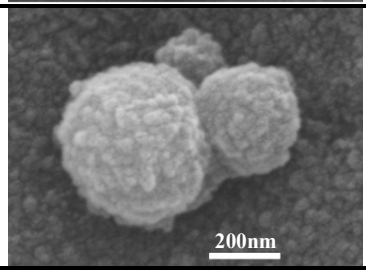
6R5 Regular	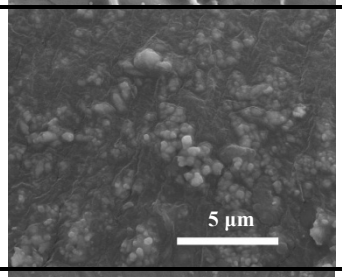	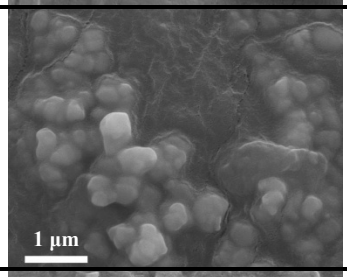	
6R5 Glycerol	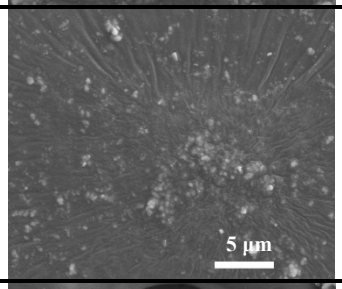	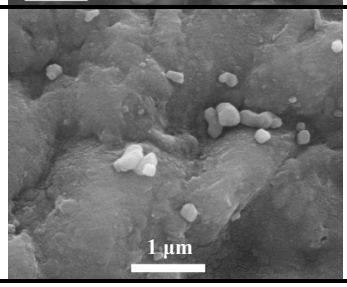	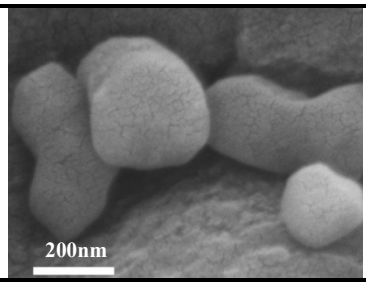
15R5 Regular	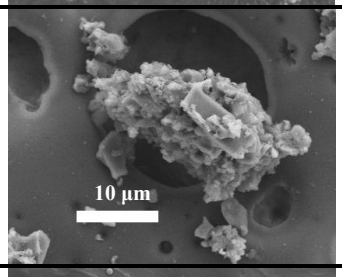		
15R5 Glycerol	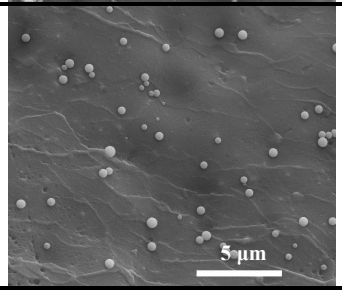	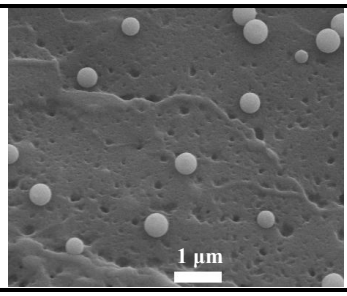	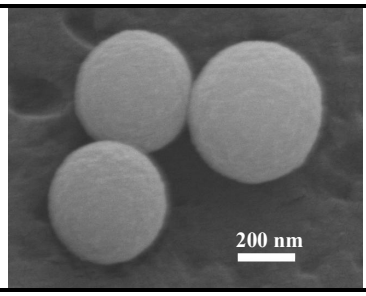

`

Appendix A2. Representative Images for Material Characterization on TCP

6mer	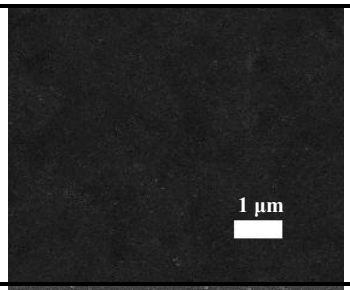		
6A3	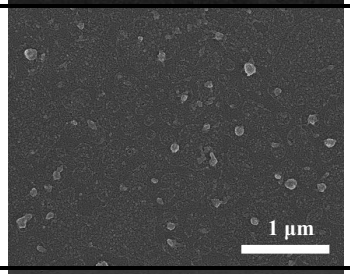	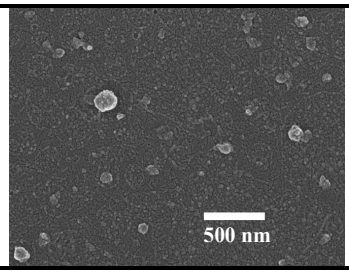	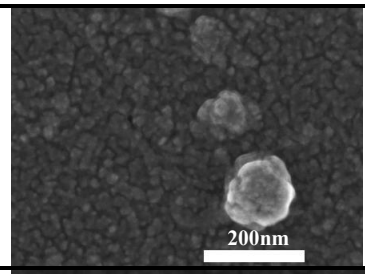
6R5	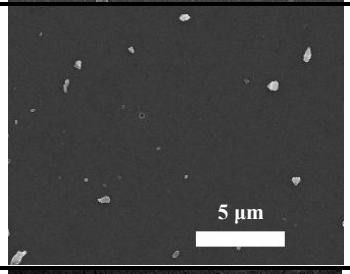		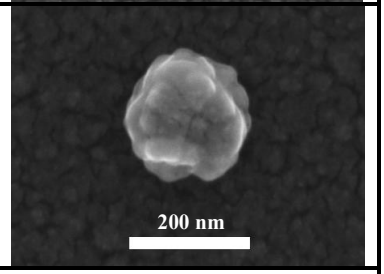
15mer	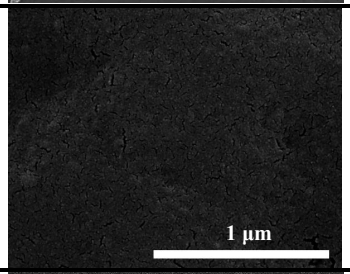		
15A3	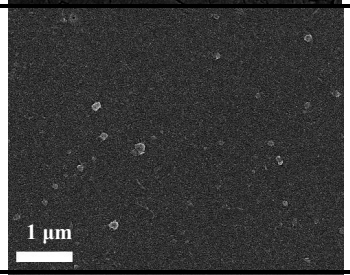	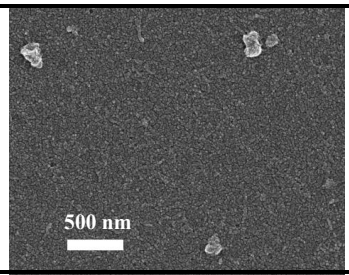	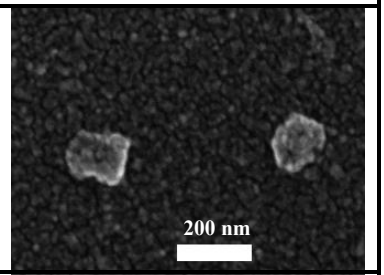
15R5	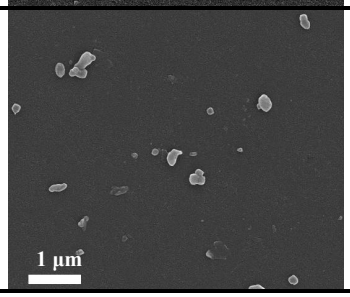	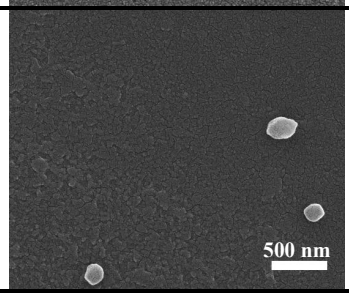	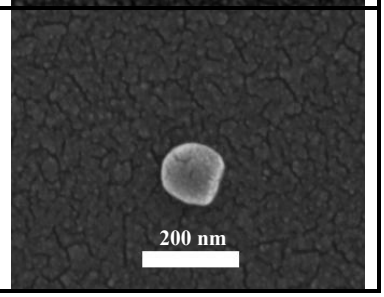

`

Appendix A3. Representative Images for Material Deposition after Cell Study

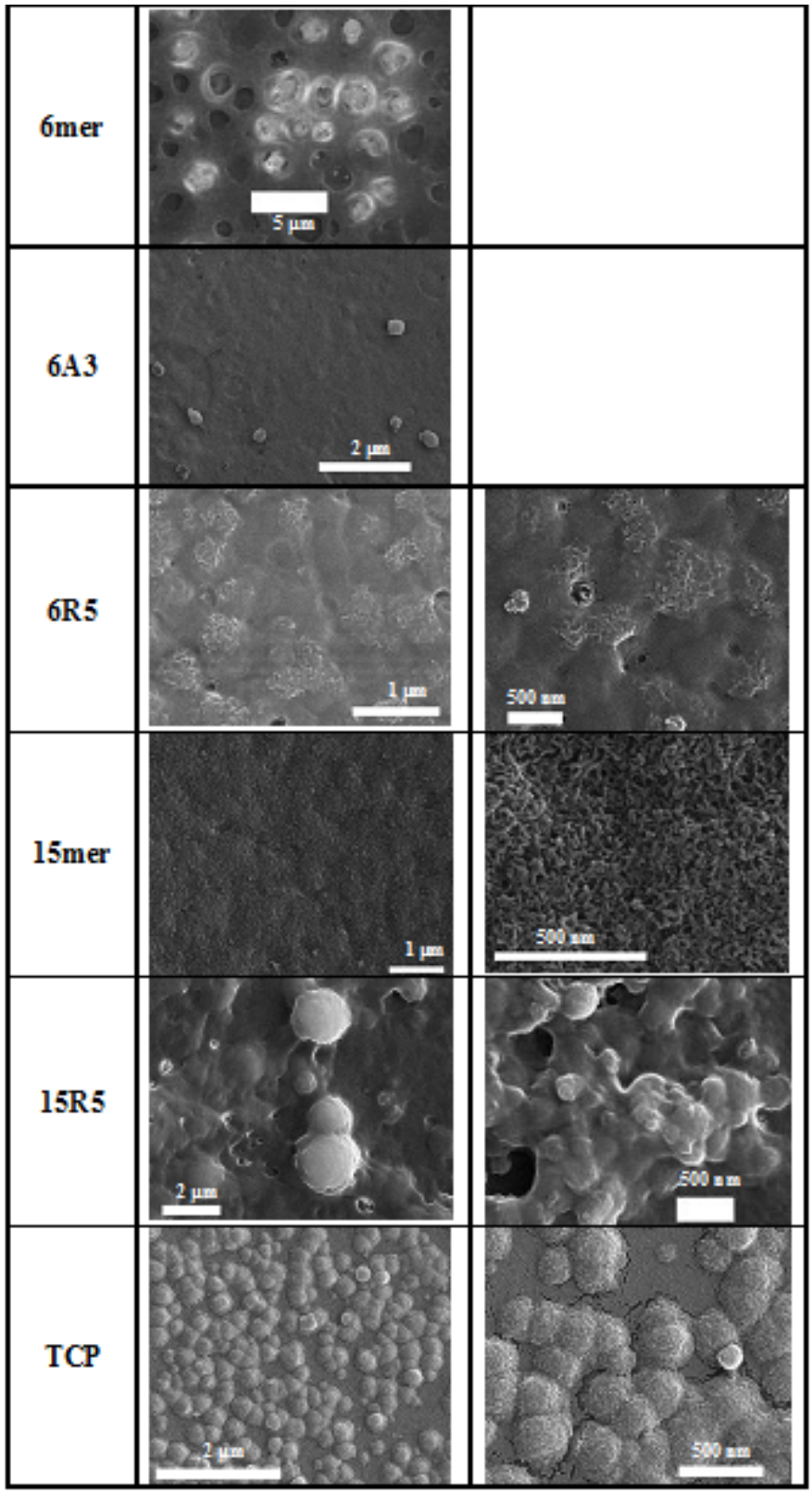

`

Appendix B: Light Microscopy Images

Appendix B1. Representative Images of Cells at Attachment and d2 Differentiation

note: scale bars are 100 μm

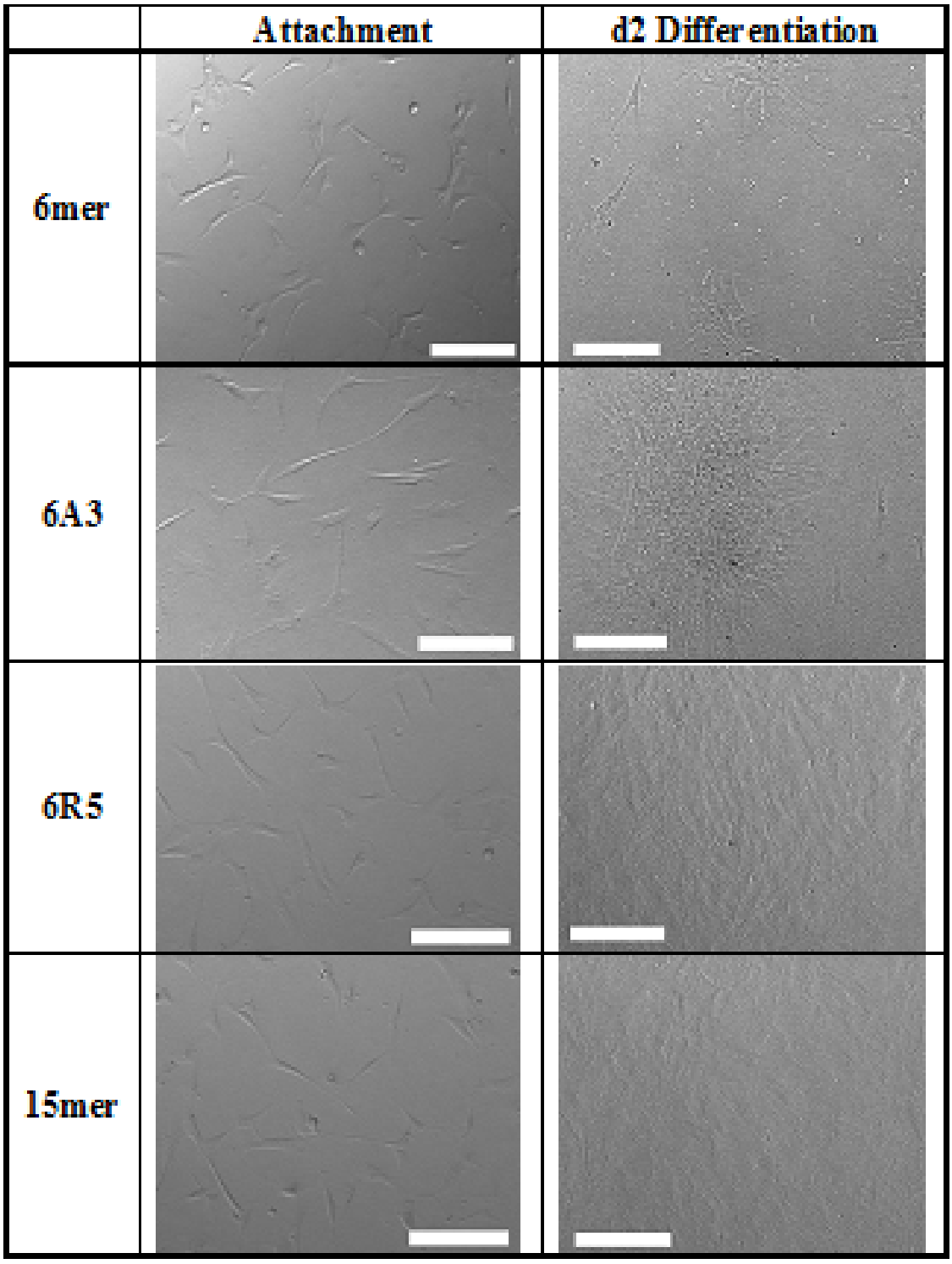

`

Appendix B1. Representative Images of Cells at Attachment and d2 Differentiation (continued)

note: scale bars are 100 μm

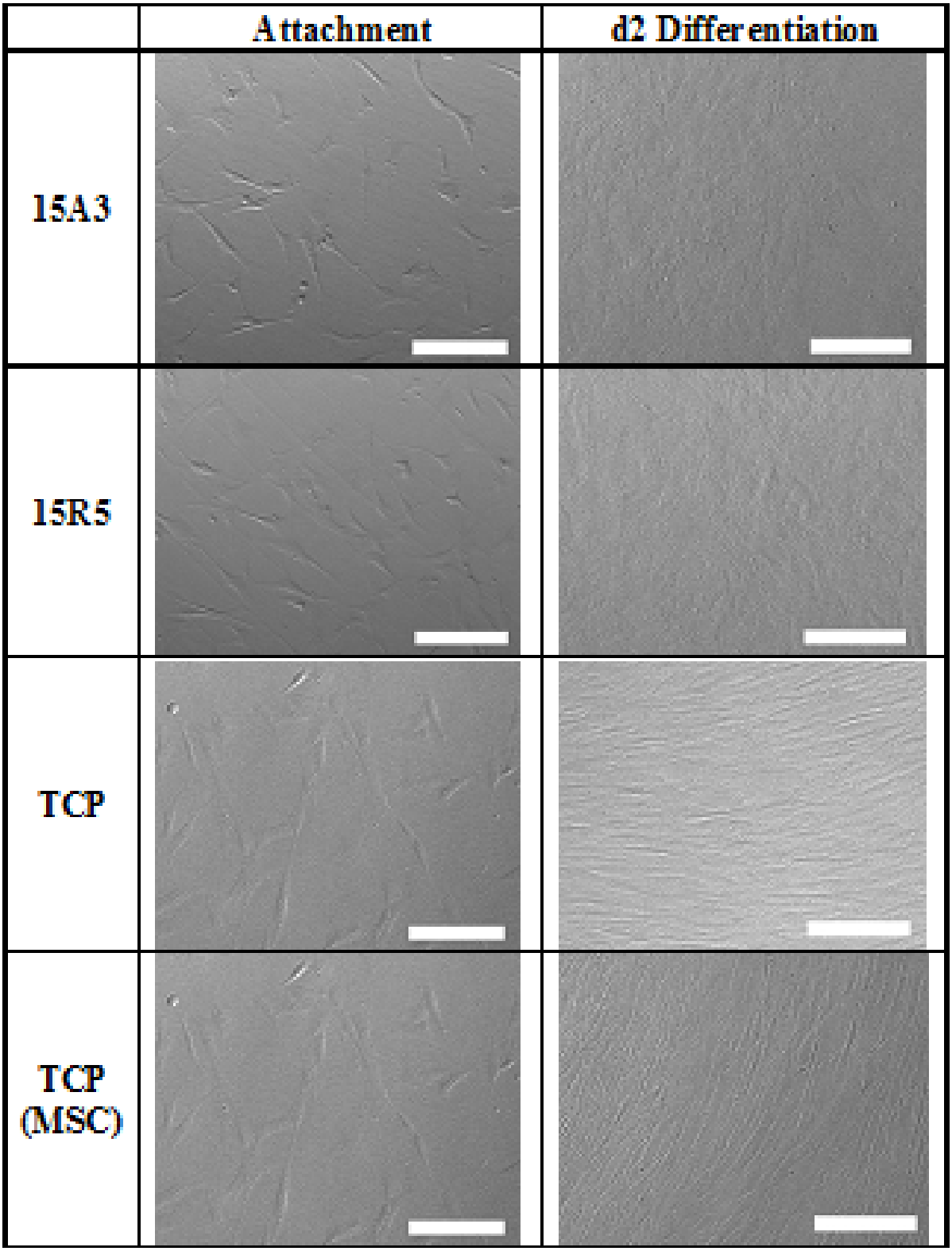

`

Appendix B2. Representative Images of Cells at Week 1 and Week 2 Assays

note: scale bars are 100 μm

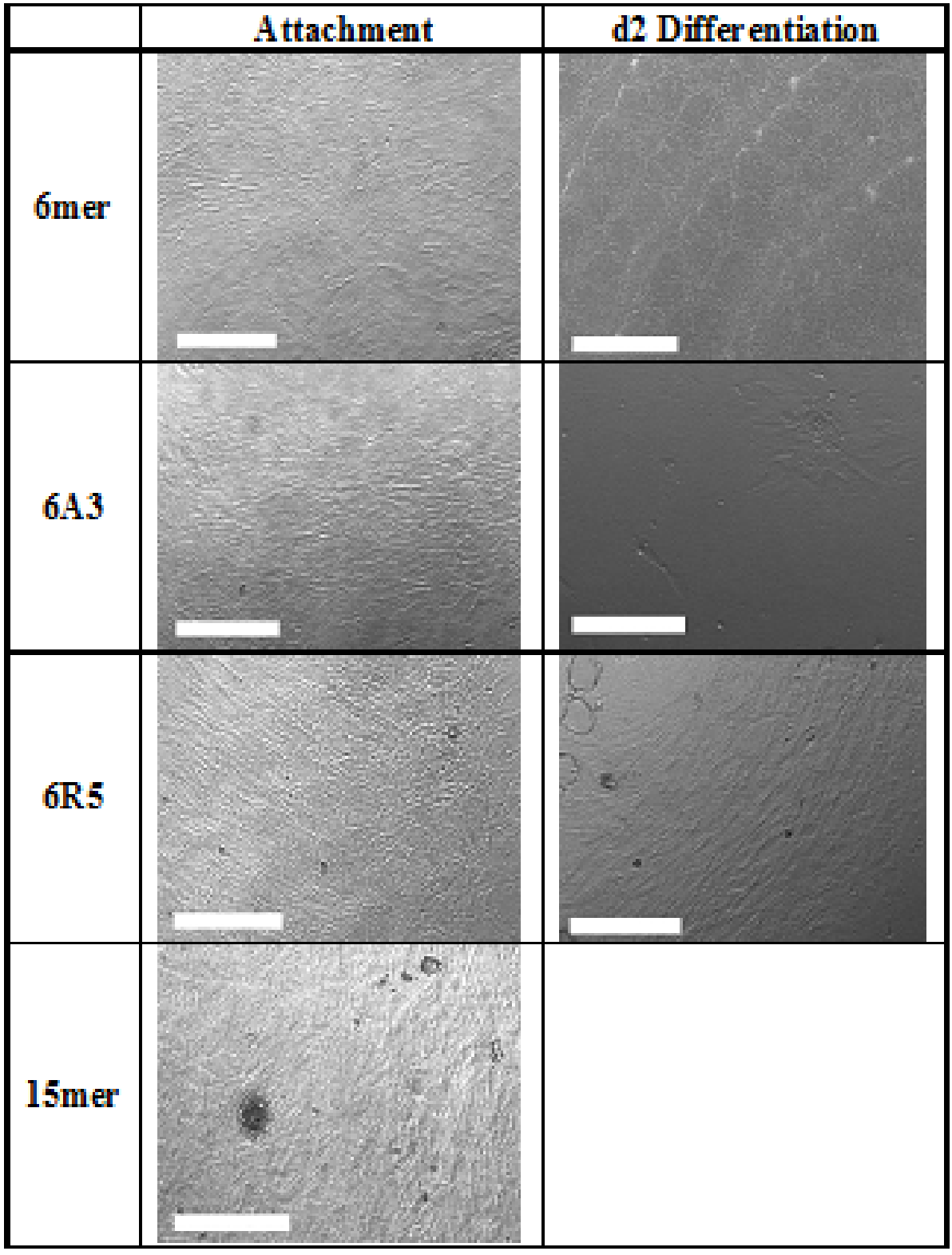

`

Appendix B2. Representative Images of Cells at Week 1 and Week 2 Assays (continued)

note: scale bars are 100 μm

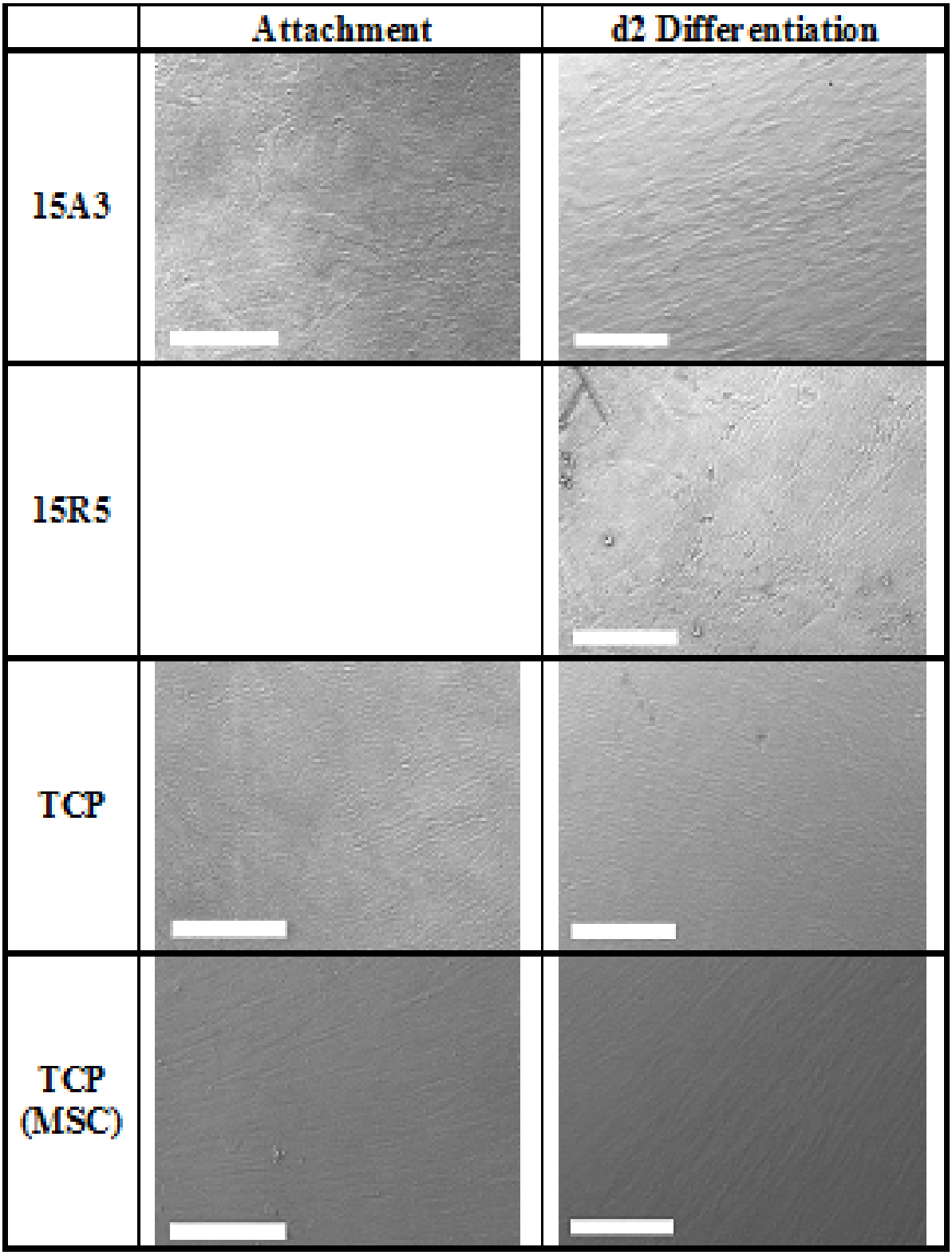

`

Appendix C: Representative EDAX Spectra and Elemental Composition

Surface	EDAX Spectrum	Atomic Composition
6mer	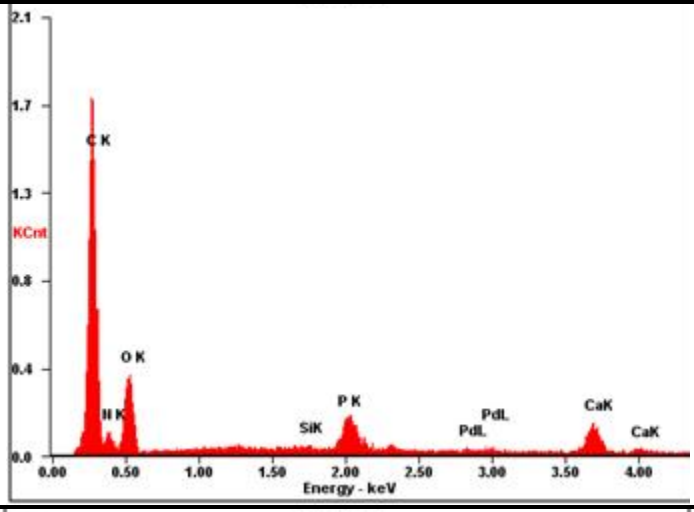	
6A3	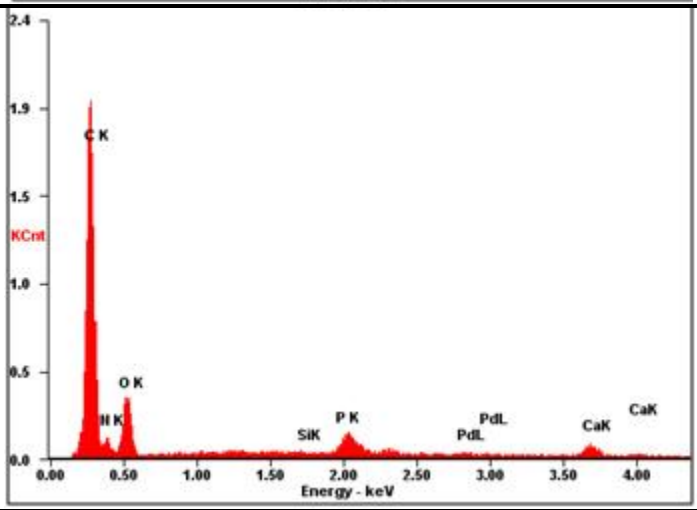	
6R5	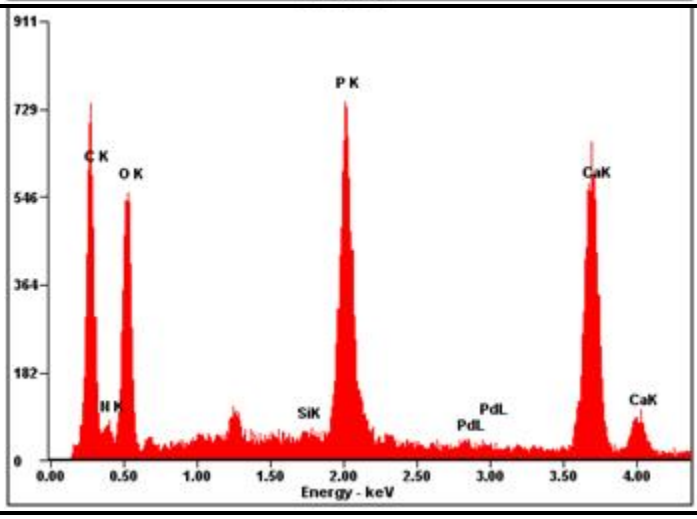	

Element	Wt %	At %
C K	47.38	63.85
N K	11.40	13.18
O K	18.06	18.27
SiK	00.18	00.11
P K	02.78	01.45
PdL	00.80	00.12
CaK	04.40	01.78
PtL	15.00	01.24

Element	Wt %	At %
C K	53.00	68.55
N K	11.79	13.08
O K	15.87	15.41
SiK	00.00	00.00
P K	01.80	00.90
PdL	00.79	00.11
CaK	02.00	00.78
PtL	14.75	01.17

Element	Wt %	At %
C K	25.36	42.60
N K	07.21	10.38
O K	23.76	29.97
SiK	00.12	00.09
P K	09.70	06.32
PdL	00.99	00.19
CaK	17.64	08.88
PtL	15.21	01.57

`

Appendix C: Representative EDAX spectra and elemental composition (continued)

Surface	EDAX Spectrum	Atomic Composition
15mer	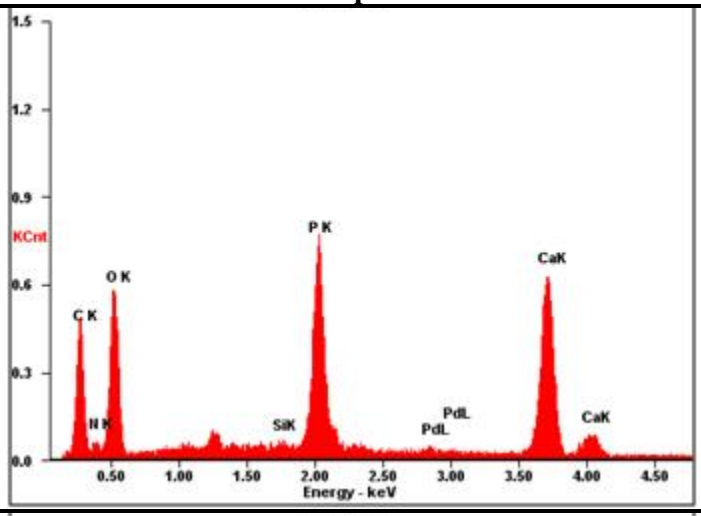	*Element* / *Wt %* / *At %* *C K* 20.79 36.61 *N K* 05.56 08.39 *O K* 26.25 34.71 *SiK* 00.36 00.27 *P K* 11.20 07.65 *PdL* 00.87 00.17 *CaK* 20.03 10.57 *PtL* 14.94 01.62
15R5	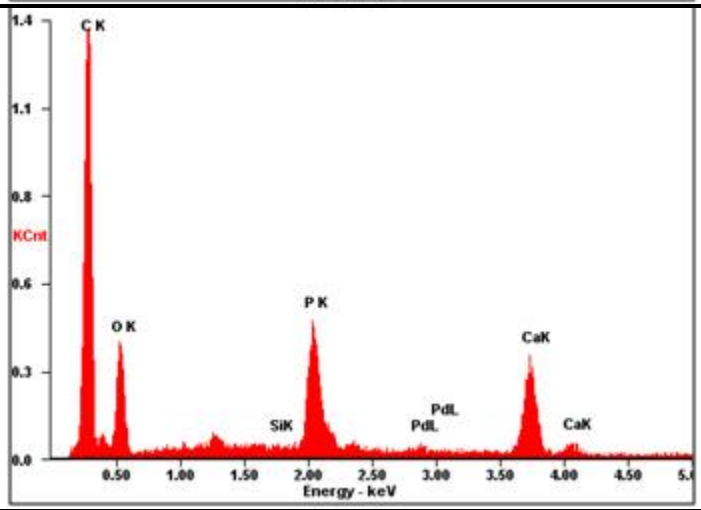	*Element* / *Wt %* / *At %* *C K* 49.96 72.38 *O K* 16.87 18.35 *SiK* 00.08 00.05 *P K* 06.27 03.52 *PdL* 00.94 00.15 *CaK* 09.40 04.08 *PtL* 16.47 01.47
TCP	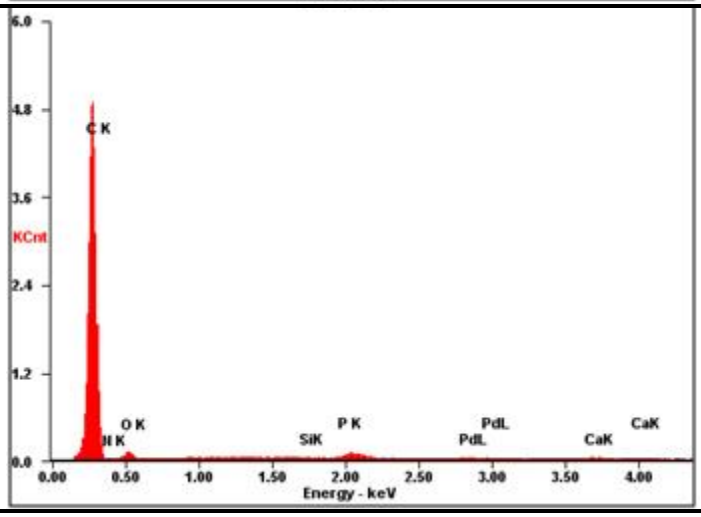	*Element* / *Wt %* / *At %* *C K* 82.10 94.13 *N K* 01.03 01.01 *O K* 03.95 03.40 *SiK* 00.00 00.00 *P K* 00.86 00.38 *PdL* 00.96 00.12 *CaK* 00.62 00.21 *PtL* 10.49 00.74

`

References:

1. American Association of Endodontists, 2008. "References." <http://www.aae.org/patients/patientinfo/references/>, accessed April 4, 2008.
2. Bowers, K.T., J.C. Keller, B.A. Randolph, D.G. Wick, and C.M. Michaels, 1992. Optimization of surface morphology for enhanced osteoblast responses *in vitro*. *The International Journal of Oral and Maxillofacial Implants*, 7(3): 302-310.
3. Cha, J.N., G.D. Stucky, D.E. Morse, and T.J. Deming, 2000. Biomimetic synthesis of ordered silica structures mediated by block copolypeptides. *Nature*, 403: 289-292.
4. Chen, J., G.H. Altman, V. Karageorgiou, R. Horan, A. Collette, V. Volloch, T. Colabro, and
5. D.L. Kaplan, 2003. Human bone marrow stromal cell and ligament fibroblast responses on RGD-modified silk fibers. *Journal of Biomedical Materials Research*, 67A(2): 559-570.
6. Duailibi, S.E., M.T. Duailibi, J.P. Vacanti, and P.C. Yelick, 2005. Prospects for tooth regeneration. *Periodontology 2000*, 41: 177-187.
7. Foo, C.W.P., J. Huang, and D.L. Kaplan, 2004. Lessons from seashells: silica mineralization via protein templating. *Trends in Biotechnology*, 22(11): 577-585.
8. Foo, C.W.P., S.V. Patwardhan, D.J. Belton, B. Kitchel, D. Anastasiades, J. Huang, R.R. Naik, C.C. Perry, and D.L. Kaplan, 2006. Novel nanocomposites from spider silk-silica fusion (chimeric) proteins. *PNAS*, 103(25): 9428-9433.
9. Gajjeraman, S., K. Narayanan, J. Hao, C. Qin, and A. George, 2007. Matrix macromolecules in hard tissues control the nucleation and hierarchical assembly of hydroxyapatite. *The Journal of Biological Chemistry*, 282(2): 1193-1204.
10. Goldberg, M. and A.J. Smith, 2004. Cells and extracellular matrices of dentin and pulp: a

biological basis for repair and tissue engineering. *Critical Reviews in Oral Biology and Medicine*, 15(1): 13-27.

11. Jin, H-J., J. Chen, V. Karageorgiou, G.H. Altman, and D.L. Kaplan, 2004. Human bone marrow stromal cell responses on electrospun silk fibroin mats. *Biomaterials*, 25: 1039-1047.

12. Kaplan, D., 2006. NIH Silica Application (R01 DE017207-01A1)

13. Kim, H.J., U-J. Kim, G. Vunjak-Novakovic, B-H. Min, and D.L. Kaplan, 2005. Influence of macroporous protein scaffolds on bone tissue engineering from bone marrow stem cells. *Biomaterials*, 26(21): 4442-4452.

14. Knecht, M.R. and D.W. Wright, 2003. Functional analysis of the biomimetic silica precipitating activity of the R5 peptide from *Cylindrotheca fusiformis*. *Chemical Communications*, 24: 3038-3039.

15. Kröger, N., S. Lorenz, E. Brunner, and M. Sumper, 2002. Self-assembly of highly phosphorylated silaffins and their function in biosilica morphogenesis. *Science*, 298: 584-586.

16. Lopez, P.J., J. Desclés, A.E. Allen, and C. Bowler, 2005. Prospects in diatom research. *Current Opinion in Biotechnology*, 16(2): 180-186.

17. Marolt, D., A. Augst, L.E. Freed, C. Vepari, R. Fajardo, N. Patel, M. Gray, M. Farley, D. Kaplan, and G. Vunjak-Novakovic, 2006. Bone and cartilage tissue constructs grown using human bone marrow stromal cells, silk scaffolds and rotating bioreactors. *Biomaterials*, 27: 6138-6149.

18. Mauth, C., A. Huwig, U. Graf-Hausner, and J-F. Roulet, 2007. Restorative Applications for

Dental Pulp Therapy. [ed.] N. Ashammakhi, R. Reis, and E. Chiellini. *Topics in Tissue Engineering*, 3(3): 1-32.

19. Meinel, L., R. Fajardo, S. Hofmann, R. Langer, J. Chen, B. Snyder, G. Vunjak-Novakovic, and D.L. Kaplan, 2005. Silk implants for the healing of critical size bone defects. *Bone*, 37(5): 688-698.

20. Meinel, L., V. Karageorgiou, R. Fajardo, B. Snyder, V. Shinde-Patil, L. Zichner, D.L. Kaplan, R. Langer, and G. Vunjak-Novakovic, 2004. Bone tissue engineering using human mesenchymal stem cells: effects of scaffold material and medium flow. *Annals of Biomedical Engineering*, 32(1): 112-122.

21. Meinel, L., V. Karageorgiou, S. Hofmann, R. Fajardo, B. Snyder, C. Li, L. Zichner, R. Langer, G. Vunjak-Novakovic, and D.L. Kaplan, 2004. Engineering bone-like tissue *in vitro* using human bone marrow stem cells and silk scaffolds. *Journal of Biomedical Materials Research Part A*, 71A(1): 25-34.

22. Mieszawska, A., D.L. Kaplan, and C. Perry, 2009. Silk/silica nanocomposites as novel biomaterials for tissue engineering. *Biophysical Journal*, 96(3): 635a.

23. Narayanan, K., R. Srinivas, A. Ramachandran, J. Hao, B. Quinn, and A. George, 2001. Differentiation of embryonic mesenchymal cells to odontoblast-like cells by overexpression of dentin matrix protein 1. *PNAS*, 98(8): 4516-4521.

24. Ndahi, H.B., 2001. Material compatibility and the human body. *The Technology Teacher*, 61(2): 19-22.

25. Oliveira, A.L., J.F. Mano, and R.L. Reis, 2003. Nature-inspired calcium phosphate coatings:

present status and novel advances in the science of mimicry. *Current Opinion in Solid State and Materials Science*, 7: 309-318.Pashley, D.H., 1996. Dynamics of the pulpo-dentin complex. *Critical Reviews in Oral Biology and Medicine*, 7(2): 104-133.

26. Perry, C.C., 2001. Silica. *Encyclopedia of Life Sciences [online]*. <http://mrw.interscience.wiley.com/emrw/9780470015902/els/article/a0002079/current/html>, accessed April 4, 2008.

27. Simon, H. (reviewer), 2006. "Health Guide." *The New York Times [online]*. <http://health.nytimes.com/health/guides/disease/periodontitis/background.html>, accessed April 4, 2008.

28. Sofia, S., M.B. McCarthy, G. Gronowicz, and D.L. Kaplan, 2001. Functionalized silk-based biomaterials for bone formation. *Journal of Biomedical Materials Research Part A*, 54(1): 139-148.

29. Wang, Y., H-J. Kim, G. Vunjak-Novakovic, and D.L. Kaplan, 2006. Stem cell-based tissue engineering with silk biomaterials. *Biomaterials*, 27: 6064-6082.

30. Wang, Y., U. Kim, D.J. Blasioli, H. Kim, and D.L. Kaplan, 2005. In vitro cartilage tissue engineering with 3D porous aqueous-derived silk scaffolds and mesenchymal stem cells. *Biomaterials*, 26: 7082-7094.

31. Ye, L., M. MacDougall, S. Zhang, Y. Xie, J. Zhang, Z. Li, Y. Lu, Y. Mishina, and J.Q. Feng, 2004. Deletion of dentin matrix protein-1 leads to a partial failure of maturation of predentin into dentin, hypomineralization, and expanded cavities of pulp and root canal during postnatal tooth development. *Journal of Biological Chemistry*, 279(18): 19141-19148.

32. Yim, E.K.F. and K.W. Leong, 2005. Significance of synthetic nanostructures in dictating

cellular response. *Nanomedicine: Nanotechnology, Biology, and Medicine*, 1: 10-21.